

# Unsteady Pressure and Velocity Measurements in Pumps

**Dr. Detlev L. Wulff**

TU Braunschweig  
Institut für Strömungsmaschinen  
Langer Kamp 6  
D-38106 Braunschweig  
GERMANY

[d.wulff@tu-bs.de](mailto:d.wulff@tu-bs.de)

## ABSTRACT

*The objective of this paper is to report the state-of-the-art of unsteady pressure measurements in pumps. Though optical techniques seem in some aspects more attracting, unsteady pressure measurements can give a detailed insight in static as well as dynamic operating behaviour of pumps. A brief description of wall mounted pressure transducers and of probes fitted with miniature pressure transducers will be given. The main topics of this report are:*

- *Miniature pressure sensors*
- *Resolution in time and space (response characteristics)*
- *Data acquisition*
- *Ensemble/phase averaging*
- *Measurements in stationary and rotating frame*
- *Detection of non-synchronous components*
- *Pressure and velocity measurements by means of high response probes (2D and 3D)*

## 1.0 INTRODUCTION

Modern design methods like CFD give detailed insight into the flow through turbo machinery. Some years ago when CFD became popular many people thought measurements would become dispensable. Today we know, it is not. Indeed, we have a growing demand for detailed measurements of the flow in turbo machinery to compare this to the obtained CFD results. Particularly with regard to the calculation of losses and efficiency pressure measurements are indispensable. Unsteady pressure measurements are widely used to examine the unsteady behaviour of pumps, for example part load pumping or operation under cavitation. Unsteady pressure measurements are carried out in the field of research as well as condition monitoring. Wall mounted pressure sensors are used for the investigation of stator and rotor flow near casing walls (Fig. 1, b and c). Measurements of pressure distribution on rotor blades are carried out with miniature transducers and telemetry systems for data transmission from rotating rotor to stationary frame of reference. Probes fitted with miniature pressure transducers are used to examine the rotor exit flow (Fig. 2) and will give complete information on the 2D or 3D flow field including velocities and pressure distribution.

Report Documentation Page				Form Approved OMB No. 0704-0188	
Public reporting burden for the collection of information is estimated to average 1 hour per response, including the time for reviewing instructions, searching existing data sources, gathering and maintaining the data needed, and completing and reviewing the collection of information. Send comments regarding this burden estimate or any other aspect of this collection of information, including suggestions for reducing this burden, to Washington Headquarters Services, Directorate for Information Operations and Reports, 1215 Jefferson Davis Highway, Suite 1204, Arlington VA 22202-4302. Respondents should be aware that notwithstanding any other provision of law, no person shall be subject to a penalty for failing to comply with a collection of information if it does not display a currently valid OMB control number.					
1. REPORT DATE <b>01 NOV 2006</b>		2. REPORT TYPE <b>N/A</b>		3. DATES COVERED <b>-</b>	
4. TITLE AND SUBTITLE <b>Unsteady Pressure and Velocity Measurements in Pumps</b>				5a. CONTRACT NUMBER	
				5b. GRANT NUMBER	
				5c. PROGRAM ELEMENT NUMBER	
6. AUTHOR(S)				5d. PROJECT NUMBER	
				5e. TASK NUMBER	
				5f. WORK UNIT NUMBER	
7. PERFORMING ORGANIZATION NAME(S) AND ADDRESS(ES) <b>TU Braunschweig Institut für Strömungsmaschinen Langer Kamp 6 D-38106 Braunschweig GERMANY</b>				8. PERFORMING ORGANIZATION REPORT NUMBER	
9. SPONSORING/MONITORING AGENCY NAME(S) AND ADDRESS(ES)				10. SPONSOR/MONITOR'S ACRONYM(S)	
				11. SPONSOR/MONITOR'S REPORT NUMBER(S)	
12. DISTRIBUTION/AVAILABILITY STATEMENT <b>Approved for public release, distribution unlimited</b>					
13. SUPPLEMENTARY NOTES <b>See also ADM002051., The original document contains color images.</b>					
14. ABSTRACT					
15. SUBJECT TERMS					
16. SECURITY CLASSIFICATION OF:			17. LIMITATION OF ABSTRACT <b>UU</b>	18. NUMBER OF PAGES <b>34</b>	19a. NAME OF RESPONSIBLE PERSON
a. REPORT <b>unclassified</b>	b. ABSTRACT <b>unclassified</b>	c. THIS PAGE <b>unclassified</b>			

## Unsteady Pressure and Velocity Measurements in Pumps

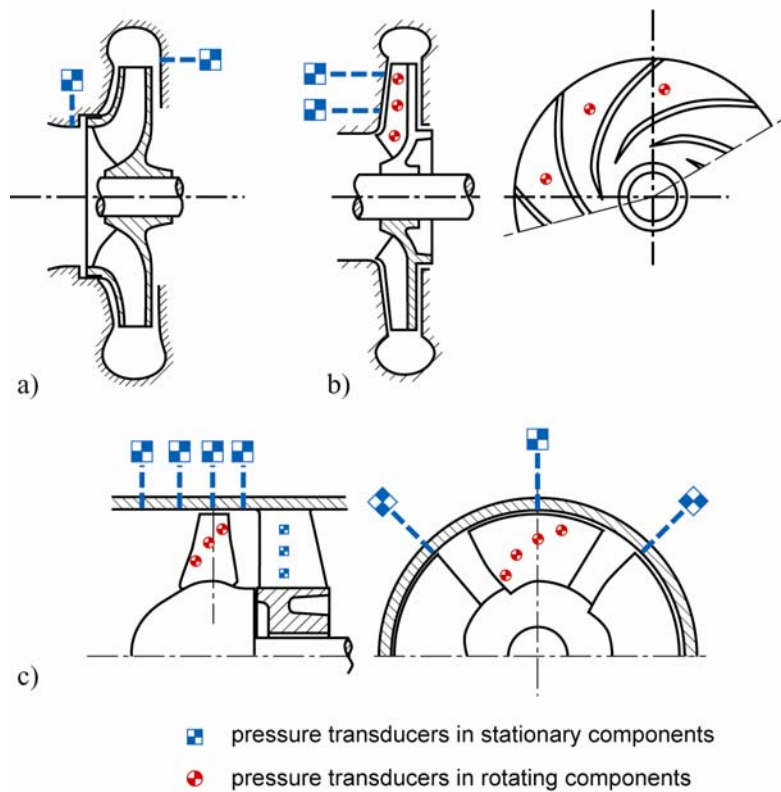


**Figure 1: Unsteady Pressure Measurements by Means of Pressure Sensors Mounted in Stationary and in Rotating Components.**

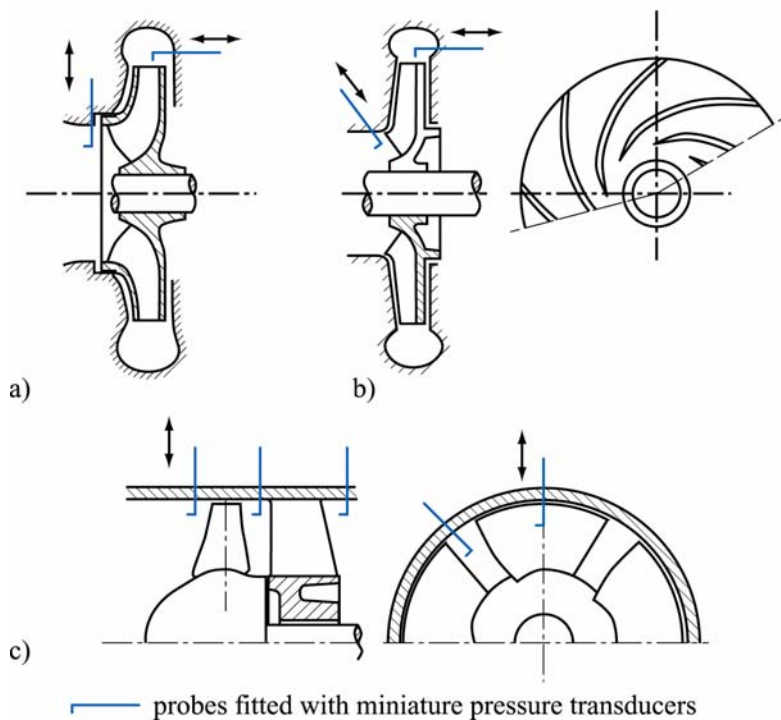


**Figure 2: Measurement of Rotor Flow using High Response Probes.**

## 2.0 SENSORS FOR UNSTEADY PRESSURE MEASUREMENTS

### 2.1 Design

Since electronic data acquisition is common practice today, electrical signals proportional to the measured pressure become essential. These signals can be generated by electromechanical pressure transducers. When pressure is applied, the force on the sensing element due to the pressure results in a deformation of the sensing element. This deformation changes the electrical properties of the element and therefore the electrical output of the sensor. Sensors for unsteady pressure measurements need a high natural frequency. Fig. 3 shows the idealized frequency response of a pressure transducer, the output is essentially independent of frequency below one-fifth of the resonance frequency [7]. Generally, a high natural frequency is achieved with small sensors with low mass and front-sided diaphragm.

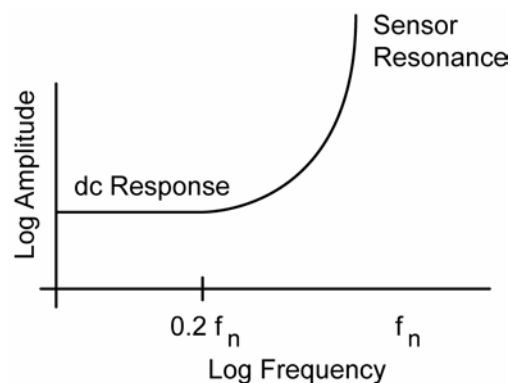


Figure 3: Idealized System Frequency Response.

Fig. 4 compares the size of a common pressure transducer suited for steady measurements with a miniature transducer for unsteady pressure measurements. The natural frequency of the common transducers is in the range of 100 Hz while the miniature transducers is around 100,000 Hz (rising with increasing pressure range, see table 1). Miniature pressure transducers are commonly available with three pressure options: gage, absolute and differential. While in common transducers metal strain gages are used, in miniature transducers silicon semiconductor bridges are employed, therefore these are called piezoresistive transducers. Advantages of the latter are: lower weight, smaller size, higher sensitivity and higher frequency response. The primary disadvantages are greater thermal sensitivity and zero shift. Fig. 5 shows a typical layout of a silicon semiconductor bridge. Most piezoresistive transducers on the market employ a fully active Wheatstone bridge consisting of four gages, which are diffused, in a silicon diaphragm. The silicon integrated chip is itself the diaphragm. Therefore a protection against the measured fluid is necessary. While for short-time service in water a coating is sufficient, for long-time service a welded steel diaphragm is advisable. The rear side of transducer is commonly sealed with epoxy that will give no adequate sealing against water intrusion. Therefore standard transducers cannot be submerged in water without damage. Fig. 7 shows a transducer with custom-made tube fitting on the rear side to provide watertight long-time service. Installation in an impeller is shown in Fig. 8, tubing on the rear side is required for routing sensor cables to amplifier and telemetry.



**Figure 4: Pressure Sensors with Four-Arm (Wheatstone) Bridge for Steady (LUCAS SCAEVITZ, top) and Unsteady (KULITE, bottom) Pressure Measurements. Battery (middle) to compare size.**

**Table 1: Specification of KULITE<sup>®</sup> XTM-Type Piezoresistive Pressure Transducer with Steel Diaphragm**

Pressure Range	1,7 bar	7 bar	35 bar
Input Impedance	650 Ohms		
Output Impedance	1000 Ohms		
Sensitivity (FSO)	7,5mV/V		
Natural Frequency	75 kHz	125 kHz	300 kHz
Residual Unbalance	$\pm 3\%$ FSO		
Combined Non-Linearity and Hysteresis	$< \pm 0,5\%$ FSO		
Thermal Zero Shift	$\pm 2\%$ FSO		

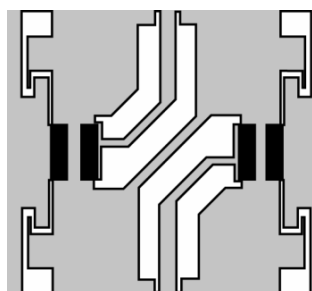


**Figure 5: Layout of Four-Arm Bridge of Piezoresistive Pressure Sensor.**

All strain gage and piezoresistive transducers are passive devices and require an external excitation (Fig. 6) to provide an output signal. The energy sources must be stable and well regulated to avoid error signals at the output. The excitation causes a finite current to flow through the bridge, which results in an increase in temperature. Water will assure good heat conduction, so this effect can in most cases be

neglected. Common power sources are DC or AC carrier power supplies. In most cases DC power supplies are preferred because of their higher frequency response.

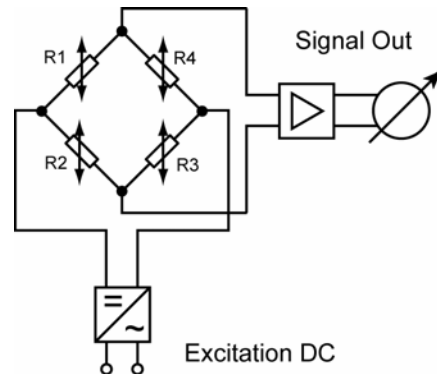


Figure 6: Schematic Diagram of Full Bridge Transducer with AC-Amplifier.

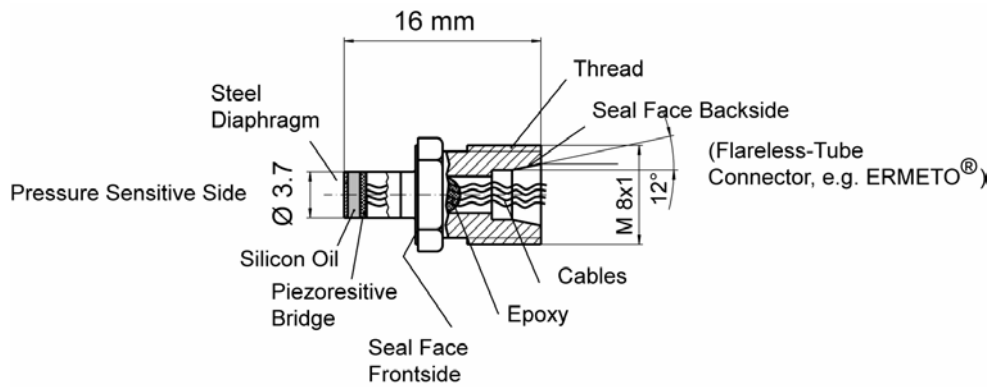


Figure 7: Piezoresistive Transducer with Custom Made Sealing on Back (KULITE® XTM-XX-190M).

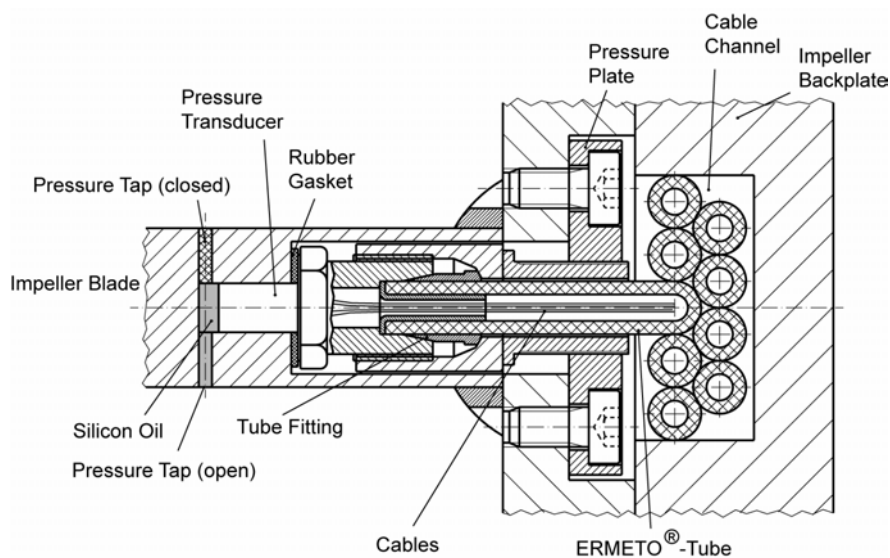


Figure 8: Piezoresistive Transducer (KULITE® XTM-XX-190M) Fitted in Pump Impeller.

If only information on the unsteady component of pressure is required, piezoelectric sensors can be used. Unlike strain gage transducers, piezoelectric devices require no external excitation. Because their output signal levels are low, special signal conditioning (charge amplifier) is required. Since measurements on pumps often deal with cavitation and therefore information on absolute pressure is required, piezoresistive transducer will be the common choice.

### 2.2 Response Characteristics

In any dynamic measurement, the frequency response of the transducer and the data acquisition system must be considered. The essential requirement to pressure measurements is that one must consider the fluid coupling to the transducer from the measuring point. A transducer mounted flush with the wall (Fig. 9a) will give the highest frequency response while installation according to Fig. 9c) can severely limit the response of the system. On the other hand an installation according to Fig. 9c will give better spatial resolution than a flush-mounted transducer. Obviously there is a trade-off between spatial and temporal resolution.

#### 2.2.1 Sonic Speed

Sonic speed of a free propagating wave in a liquid is:

$$a = \sqrt{\frac{E}{\rho}}$$

where  $E$  = volume modulus [N/m<sup>2</sup>]  
 $\rho$  = mass density [kg/m<sup>3</sup>]

The approximate speed of sound in water and air:

Water:  $a \approx 1440$  m/s  
 Air:  $a \approx 330$  m/s

A pressure line between measuring point and transducer reduce the speed of sound due to elasticity of the tube walls to

$$a'_w = \sqrt{\frac{1}{\rho_w \left( \frac{1}{E_w} + \frac{1}{E} \cdot \frac{D}{s} \right)}}$$

where  $E_w$  = [N/m<sup>2</sup>] volume modulus of water  
 $E$  = [N/m<sup>2</sup>] volume modulus of tube wall  
 $\rho_w$  = [kg/m<sup>3</sup>] mass density of water  
 $D$  = [m] tube diameter  
 $s$  = [m] wall thickness of tube

For example, the speed of sound in a tube with 4 mm inner diameter and 1 mm wall thickness is reduced:

Steel tube:  $a' \approx 1390$  m/s  
 Polyamide tube:  $a' \approx 630$  m/s

## 2.2.2 Temporal Resolution

The flush mounted transducer will give the highest frequency response while recessed installation according to b) and c) in Figure 9 will reduce system response. The following simple models will give a rough estimate of the effect. The assumptions are: viscous effects are negligible and flow is one-dimensional.

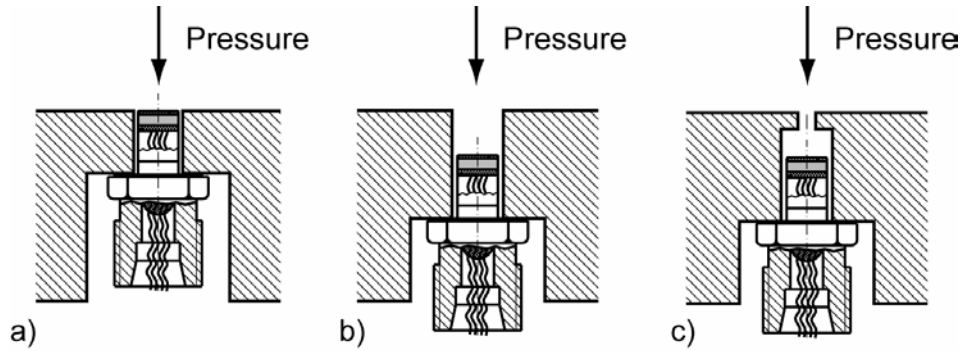


**Figure 9: Installation of Miniature Pressure Transducers.**

### *Organ Pipe Resonance*

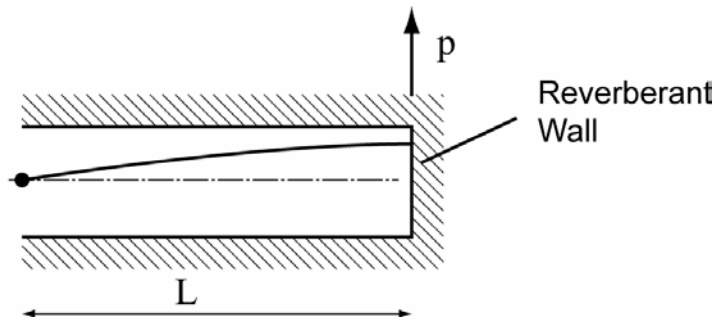


**Figure 10: Organ-Pipe Resonance.**

The wavelength of the fundamental wave is equal to four times the length of the pipe that is open at one end and closed at the other end. Resonant excitation can be produced by the fundamental frequency  $f_n$  and all the odd harmonics.

$$f_n = \frac{n}{4} \cdot \frac{a}{L} \text{ with } n = 1, 3, 5 \dots$$

where  $L$  = length of the pipe  
 $a$  = speed of sound

The wavelength  $\lambda$  is given by

$$\lambda_n = \frac{a}{f_n} = \frac{4}{n} \cdot L \text{ with } n = 1, 3, 5 \dots$$



## Helmholtz Resonance

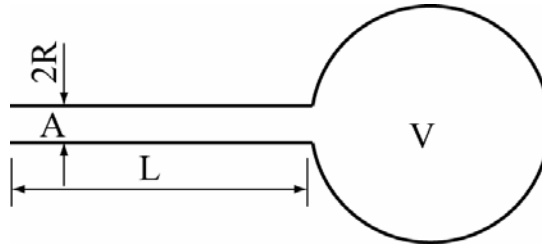


**Figure 11: Helmholtz Resonator.**

The natural frequency for a cavity connected to a pipe is given by:

$$f_0 = \frac{a}{2\pi} \sqrt{\frac{A}{V \left[ L + \frac{\pi}{2} \cdot R \right]}}$$

where      A = area of pipe  
              V = volume of cavity

## Pinhole Resonance

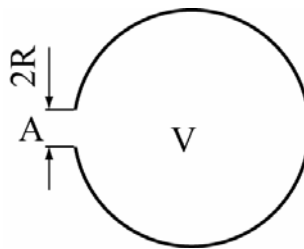


**Figure 12: Pinhole Resonance.**

If the pipe has essentially no length, such a whole in thin plate, the natural frequency is given by:

$$f_0 = \frac{a}{2\pi} \sqrt{\frac{2R}{V}}$$

### 2.2.3 Dynamic Response of Transducer in Liquid System

When pressure transmission lines become longer, the aforementioned models oversimplify the situation. The transducer force summing device may be considered as a spring, mass and damping dashpot. When this is attached to a liquid system one must effectively add liquid mass and damping to this mechanical system. Since the diameter of transmission lines is generally small, it can be assumed that friction follows Stokes flow. When doing so the resonance frequency of the measurement system is significantly lowered [7, 10]. Connections between measuring point and transducers should therefore be as short as possible. More information is given in [10].

## 2.2.4 Spatial Resolution

The wavelength  $\lambda$  of a free propagating pressure wave is given by

$$\lambda = \frac{a}{f}$$

where  $a$  [m/s] = speed of sound  
 $f$  [Hz] = wave frequency

When a pressure transducer is flush mounted to a wall it will achieve the best frequency response, but at high frequencies the wavelengths may become quite short in relation to the transducer diaphragm. According to Figure 13 an averaging of the pressure waves will occur. This can be reduced by mounting the transducer in a cavity, which is connected to the measuring point by a small hole (Fig. 13, right); drawback is the reduced natural frequency.

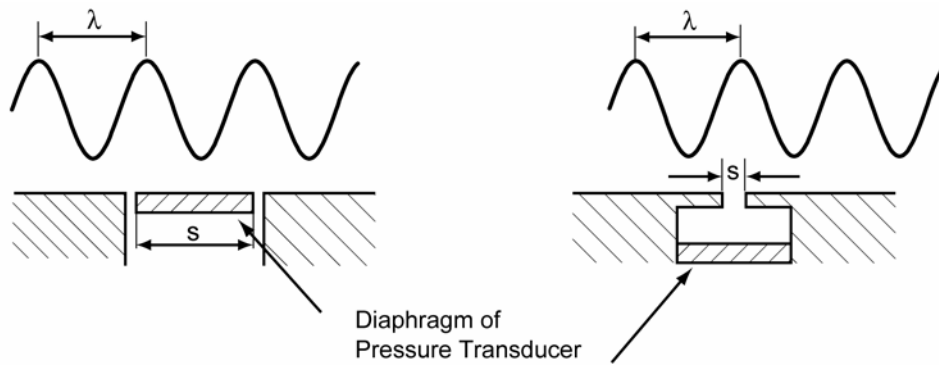


**Figure 13: Spatial Resolution (Pressure Wave Averaging).**

Attenuation of the measured pressure can be estimated for sinusoidal waves by:

$$\left| \frac{p_{out}}{p_{in}} \right| = \frac{\left| \sin \left( \pi \cdot \frac{s \cdot f}{a} \right) \right|}{\pi \cdot \frac{s \cdot f}{a}} = \frac{\left| \sin \left( \pi \cdot \frac{s}{\lambda} \right) \right|}{\pi \cdot \frac{s}{\lambda}}$$

A function of the type  $\sin(x)/x$  is also known as sinc-function. Figure 14 can be used for estimating the attenuation of measured pressure for a given transducer diameter and wavelength. For example, a transducer will give an attenuation of 10 % when the transducer diameter is four times the wave length (Fig. 14). On the other hand, for a transducer with 4 mm diameter at a frequency of 10.000 Hz (in water, sound speed  $\approx 1400$  m/s) the ratio of sensor size  $s$  to wave length is  $s/\lambda = 4/140 = 0.03$ . With the equation above this will lead to an attenuation of only 0.001.

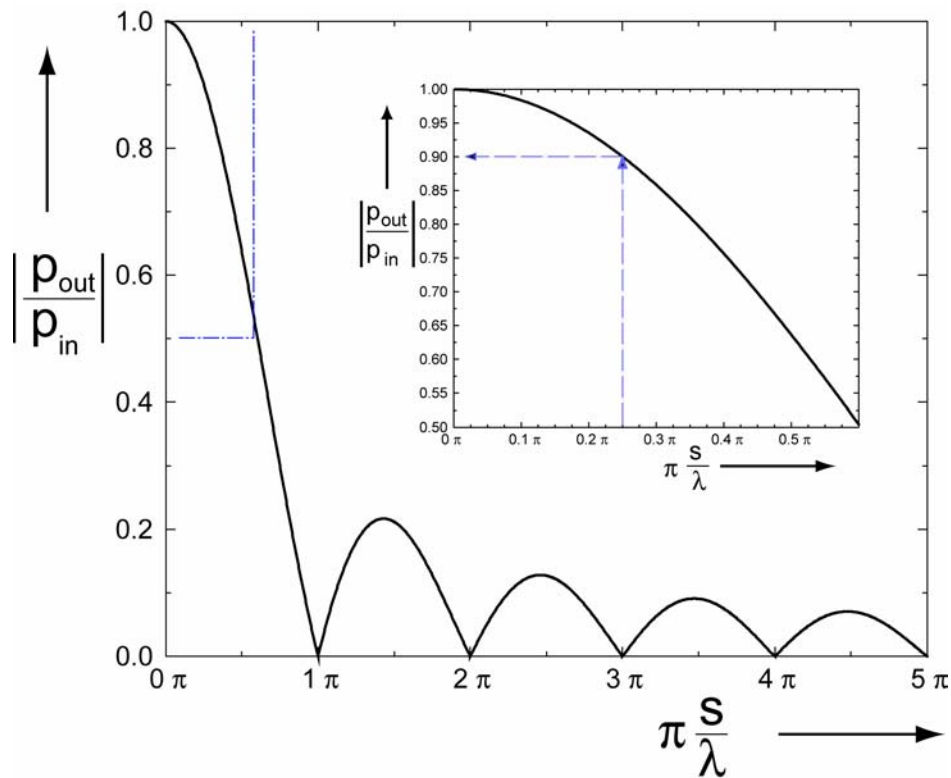


Figure 14: Attenuation of Measured Pressure versus Sensor Size (Sinc-Function).

## 2.2.5 Spatial Resolution in Rotating Frame

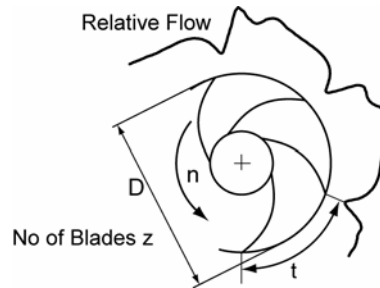


Figure 15: Pressure Signal at Rotor Exit.

The aforementioned consideration is only valid for free propagating sinusoidal waves. For example, when the exit flow of an impeller is observed from stationary frame, the pressure waves are rotating with impeller speed. The “fundamental wave length” at impeller exit is therefore determined by

$$\lambda' = \frac{u}{f_{BPF}} = \frac{\pi \cdot n \cdot D}{n \cdot z} = t$$

where

- $t [-]$  = blade pitch
- $D [m]$  = impeller outer diameter
- $u [m/s]$  = circumferential speed at outlet

Since rotor exit flow is not sinusoidal, the pressure signals will contain much higher frequencies. The blade passing frequency must therefore be replaced by a considerable higher frequency to achieve a reasonable good spatial resolution:

$$\frac{s}{\lambda''} = \frac{s \cdot f_{\max}}{u} \gg \frac{s}{\lambda'}$$

## 3.0 UNSTEADY MEASUREMENTS

The first step in the analysis of unsteady pressure measurements is a classification of the acquired data. Generally unsteady pressure measurements may be regarded as a function of time. According to Figure 16 unsteady data can be classified in deterministic and random data. Deterministic data are those that can be described by a mathematical relationship, random data can only be treated with statistical methods. From a practical point of view the decision if data are deterministic or random is usually based on the ability to reproduce the data with controlled experiments. For example, the rotor exit flow measured by means of a stationary high response probe will be periodic with a certain amount of random data caused by turbulence, noise from the measuring system and, if present, by cavitation. Full-developed rotating stall will give deterministic data, while inception of rotating stall may be regarded as random data. Cavitation itself is an example for a random process.

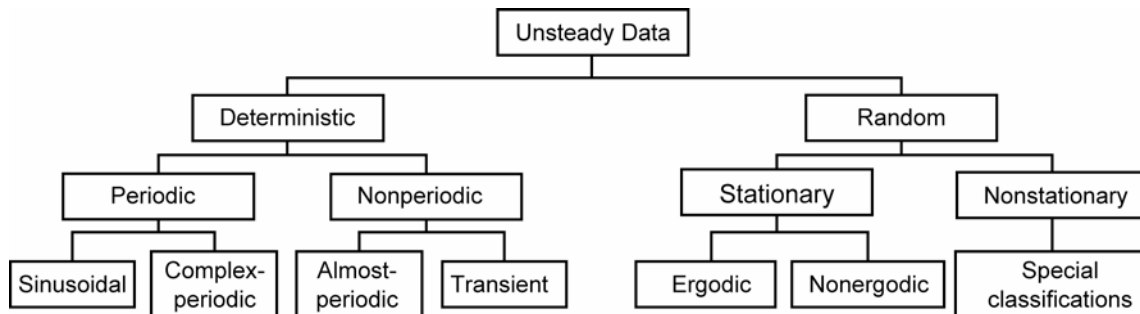


Figure 16: Classification of Unsteady Data (q.v. [1]).

## 3.1 Averaging Technique for Rotor Flow

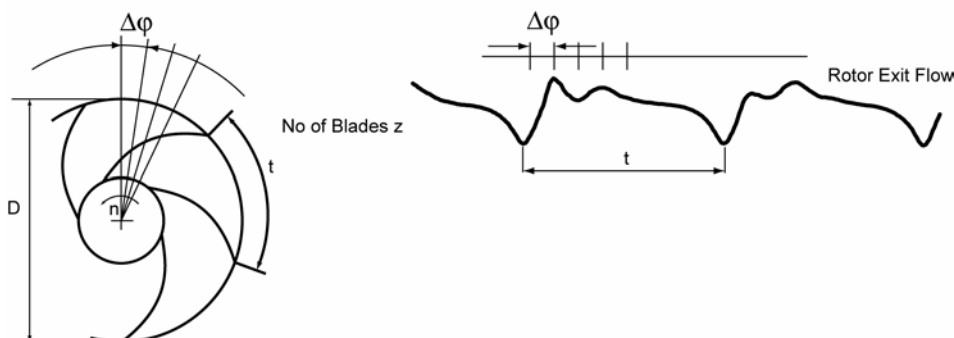


Figure 17: Spatial Resolution for Measurements of Rotor Flow.

When measurements of rotor exit flow are made in the stationary frame, spatial resolution in circumferential direction of the impeller is determined by the sampling rate.

## Unsteady Pressure and Velocity Measurements in Pumps

$$\Delta\varphi = \frac{360^\circ \cdot n}{f_{\text{Samp}}}$$

where

$n$ [1/s]	= rotor speed
$f_{\text{Samp}}$ [1/s]	= sampling rate
$\Delta\varphi$ [°]	= spatial resolution

A pressure transducer in the stationary frame near rotor inlet or outlet senses the unsteadiness that consists of both the periodic component, at the blade passing frequency, and the random component. Figure 18 shows the unsteady pressure at rotor exit measured by a miniature sensor mounted near impeller exit (Figure 1a). The time signal (Fig. 18, top) illustrates the random character while in the frequency domain the periodical character is obvious. The blade passing frequency and its harmonics can easily be detected.

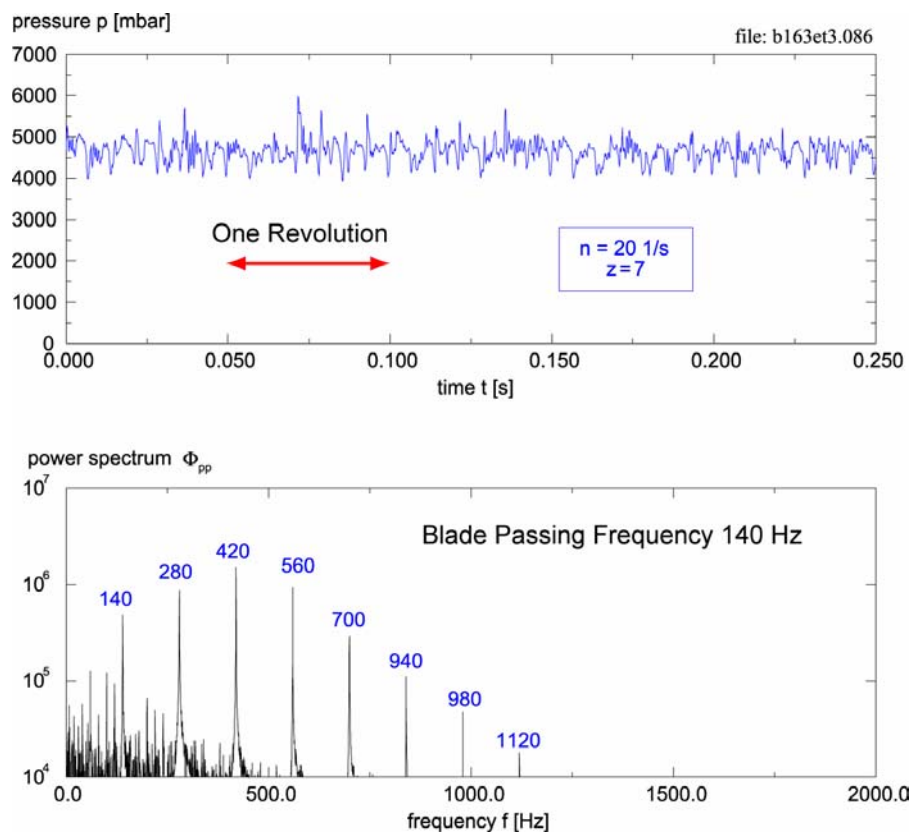


**Figure 18: Unsteady Pressure Signal at Impeller Exit (top) and Power Spectra showing Blade Passing Frequency and Higher Harmonics (bottom).**

The unsteady pressure signal can be decomposed into

$$p_u(t) = \bar{p}_u(t) + p(t)$$

where

$p_u(t)$	= measured unsteady signal
$\bar{p}_u(t)$	= periodically part of the signal
$p(t)$	= random part of the signal

To extract the information of the periodical and the random component a phase locked ensemble averaging technique [16, 17] is employed. The averaging process leads to an increase of the signal-to-noise ratio since the random component of signal will decrease with the number  $N$  of averaged data sets (see also Fig. 21).

$$\frac{\text{signal}}{\text{noise}} \sim \frac{1}{1/\sqrt{N}} = \sqrt{N}$$

For example, averaging over 100 data sets will increase the signal-to-noise ratio by a factor of ten. Combined with digital data acquisition there are the following two methods that are used for the averaging process of the rotor flow.

Method A utilizes the internal time base of the data acquisition system, at every revolution the measurement is started via a trigger signal given by a shaft encoder driven by the impeller shaft. The averaging is carried out after all data sets are recorded. The advantage of method A is that the sampling rate and number of data which are recorded can be chosen in a wide range and are only limited by the hardware used, therefore high spatial resolution can easily be obtained. Since only the first sample of each data set the measurement is actually phase locked, there may occur a phase shift between data acquisition and impeller speed which will lead to jitter in spatial resolution and accordingly to an increase in variance (Fig. 19, left).

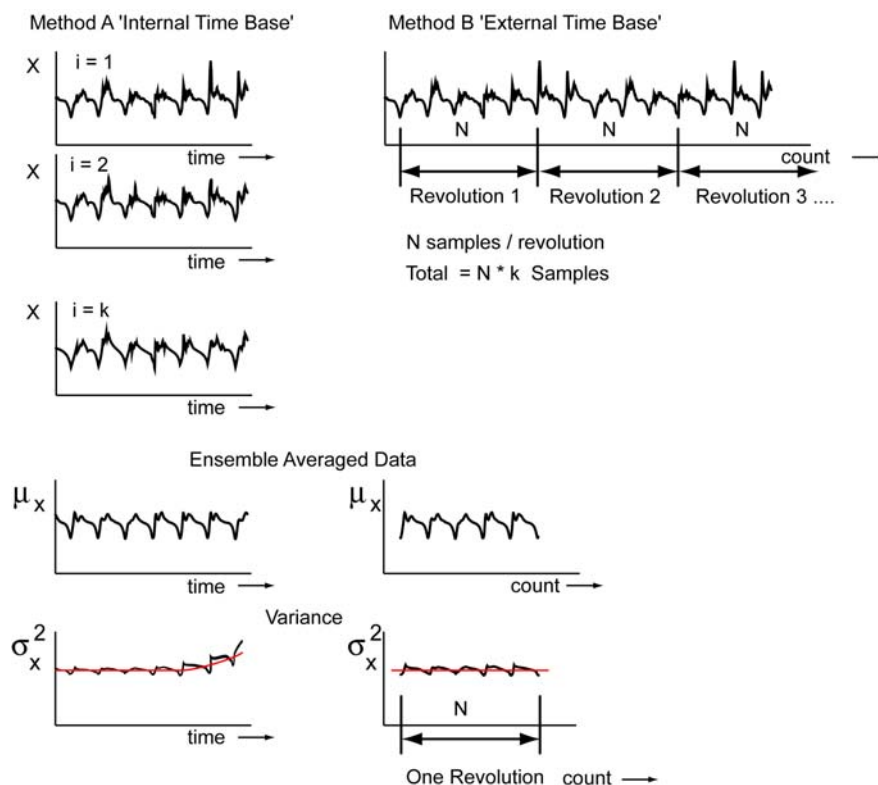


**Figure 19: Two Methods for Phase Locked Ensemble Data Averaging.**

Method B "External Time Base" requires a shaft encoder which will give additional TTL level signals which can be used as an external clock. For example, a shaft encoder with 720 pulses per revolution will give a spatial resolution of 0,5 degrees. Additionally the data acquisition system must have an input for an

## Unsteady Pressure and Velocity Measurements in Pumps

external clock. If method B is utilized the measurement is started through the trigger signal and the sampling rate is determined by

$$f_{\text{Samp}} = n \cdot c$$

where  $n$  [1/s] = impeller speed  
 $c$  [-] = pulses/revolution from shaft encoder

The advantage of method B is the real phase locking to impeller speed, therefore data acquisition is unaffected by variation of impeller speed. Drawbacks are: data sets are large, spatial resolution is determined by the shaft encoder and hardware may be more expensive.

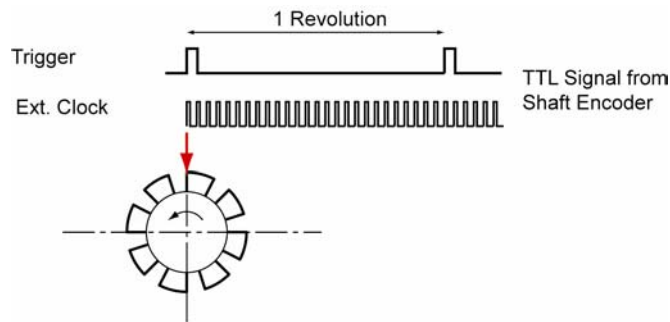


Figure 20: TTL-Signals from Shaft Encoder are Used to Control Data Acquisition.

Comparing the instantaneous signal with the averaged signal over 81 revolutions in Figure 21 demonstrates the increase in signal-to-noise ratio.

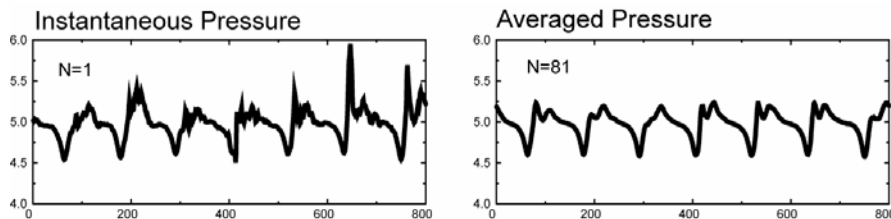
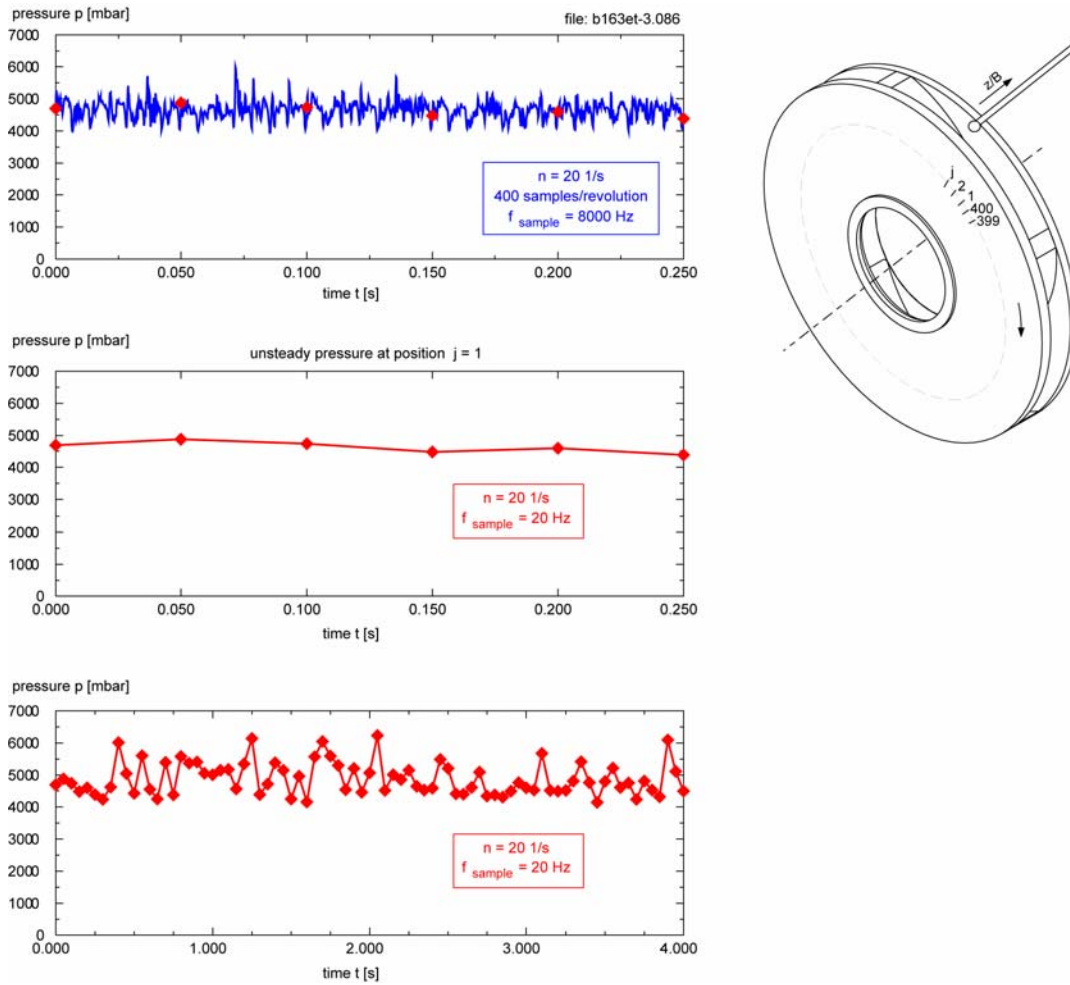


Figure 21: Instantaneous and Phase Averaged Pressure Signal at Impeller Exit.

### 3.2 Investigation of Rotor Flow from Stationary Frame

For example, the rotor exit flow is measured with a probe according to Figure 22, impeller speed  $n = 20$  1/s and shaft encoder gives 400 pulses per revolution. Thus the sampling frequency is given by

$$f_{\text{Samp}} = n \cdot c = 20 \cdot 400 = 8000 \text{ Hz}$$



**Figure 22: Unsteady Pressure at Impeller Outlet – Despite Total Sampling Rate is 8000 Hz, for Each Point at Outlet the Sampling Rate is Equal to Impeller Speed of 20 Hz.**

With respect to the *Nyquist Theorem* the highest frequency in the signal must be below the aliasing or Nyquist frequency of

$$f_a = \frac{1}{2} f_{\text{Samp}} = \frac{1}{2} 8000 = 4000 \text{ Hz.}$$

But this is only true for the time signal itself, if we want to investigate the relative flow in the rotor from the stationary frame, the sampling rate for each point in respect to impeller position is equal to impeller speed. To avoid aliasing the frequency of the rotor relative flow must therefore be below

$$f_{\text{rel}} \leq \frac{1}{2} n = 10 \text{ Hz.}$$

That means, measurement of rotor flow in stationary frame with a single sensor is more or less limited to the stationary relative flow (or periodic absolute flow). Since in most cases phase averaging is necessary to enhance signal-to-noise ratio, this will be no real restriction. Otherwise this should be kept in mind to choose the appropriate method of signal analysis.



### 3.2.1 Instrumentation for Phase Locked Measurements

A typical set-up for phase locked measurements is shown in Figure 23. Unsteady pressure is measured via wall-mounted transducers and/or high response probes, each signal is processed through a DC-amplifier, signal conditioner and aliasing filter. The shaft encoder controls data acquisition, a trigger signal starts the measurement while the sampling rate is determined by pulses generated by the shaft encoder. Simultaneous data acquisition is assured by a sample & hold device. Digitising is done by a 16-bit D/A-converter and data are stored in an internal memory. When the measurement is finished, data are read by PC high-speed data bus for final processing and storage.

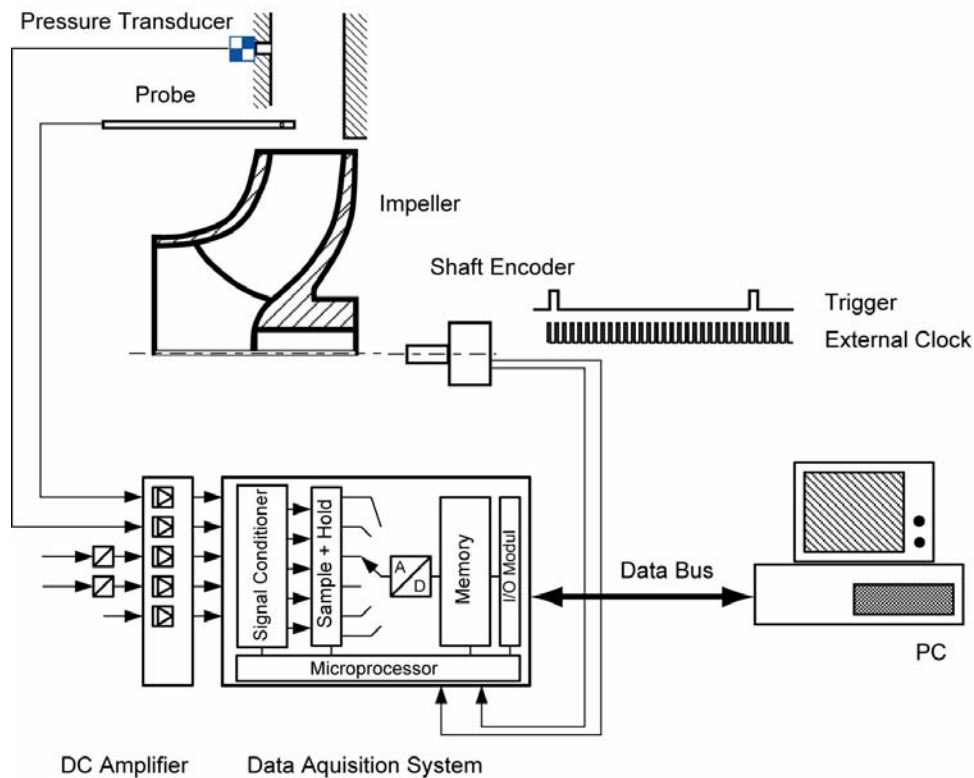


**Figure 23: Schematic of Instrumentation for Phase Locked Measurements from Stationary Frame.**

If data sets of two or more channels have to be correlated it is essential that all channels are recorded at the very same time. In many data acquisition systems two or more channels have to share one A/D-converter and must therefore be multiplexed. Since one channel after another have to be passed through to the A/D-converter this leads to a time lag according to Fig. 24. If sample and hold amplifiers for all channels are provided, the analogue data of all channels will be stored at the same time and can subsequently be digitised (Figure 23).

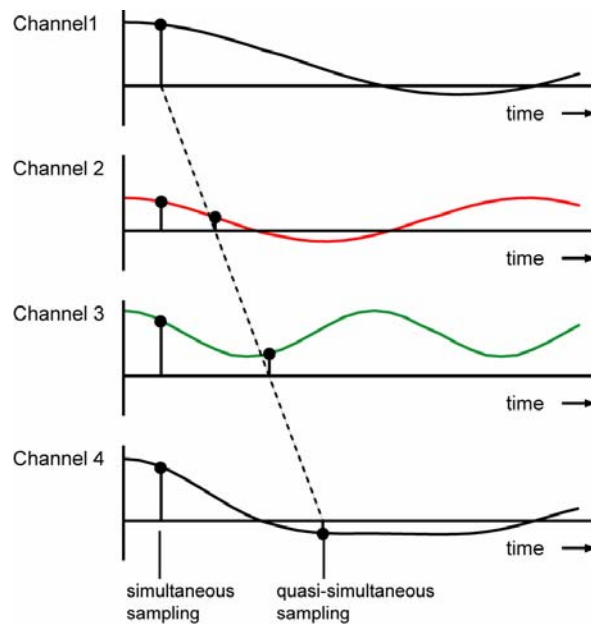


**Figure 24: Simultaneous Sampling is Assured by Means of Sample and Hold Amplifier (SSH).**

## *Example: Measurement of Blade-to-Blade Pressure Distribution Near Wall*

This example illustrates the measurement of the blade-to-blade pressure distribution near the wall of an axial flow pump. Data acquisition set-up follows up to Fig. 23. Fig. 25 shows 8 pressure transducers mounted in an insert that will fit in any of the 12 slots in the pump casing while other slots are closed by blind plates. Thus a maximum 96 measuring positions in axial direction can be enabled, multiplied with 900 measuring points in circumferential direction yields a total of  $96 \times 900 = 86400$  measuring points. Due to the inclined mounting with respect to the impeller axis the spatial resolution in axial direction is 3 mm. Spacing in circumferential direction of the measuring taps is  $8^\circ$  or with respect to employed shaft encoder with 900 counts per revolution  $8/360 \times 800 = 20$  counts. Synchronism of data is ensured by shifting the data sets by  $i \times 20$  counts ( $i=0, 1, \dots, 7$ ). Figure 27 shows the averaged reading for 5 neighboured sensors (left) and the time shifted data.

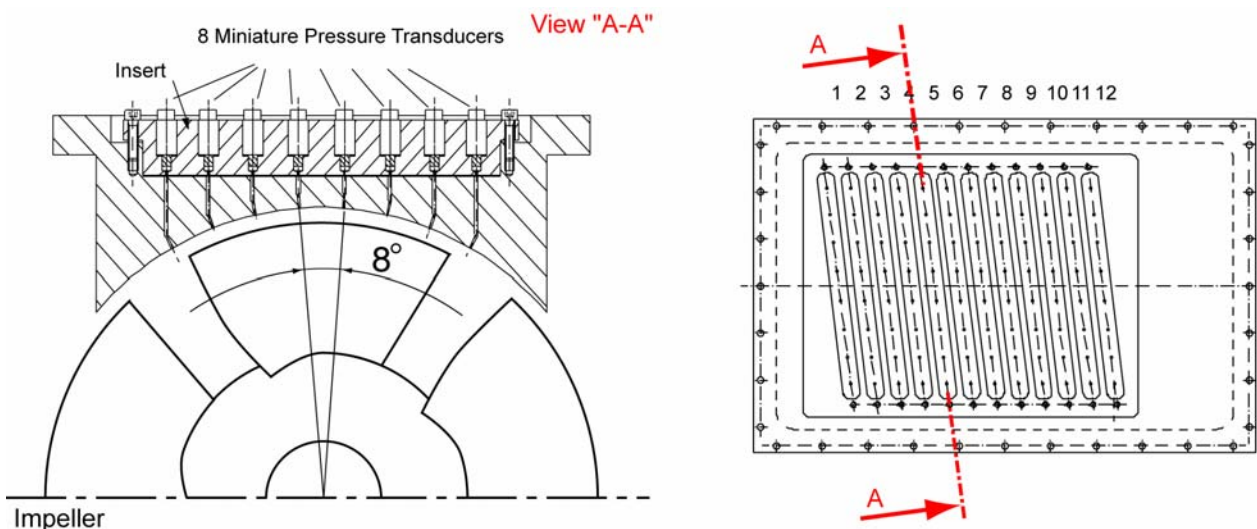


**Figure 25: Measurement of Blade-to-Blade Pressure Distribution of an Axial Flow Pump.**

## Unsteady Pressure and Velocity Measurements in Pumps

To obtain high natural frequency bleeding of all measuring taps is crucial, since remaining air will lower the systems naturally frequency dramatically. The cavity in front of the transducers is filled with silicon oil, which is proved to remain there even when inserts have to be changed for several times in different slots. Measuring holes in pump casing are filled with water from test rig.

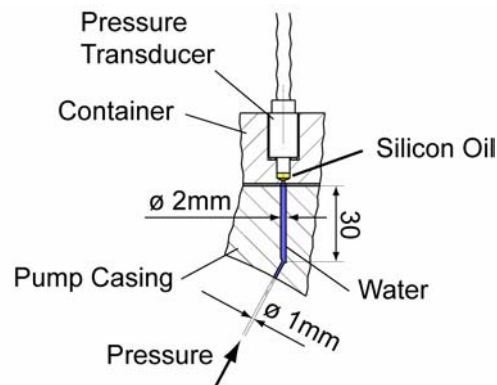


**Figure 26: Installation of Pressure Transducers (Detail to Fig. 25).**

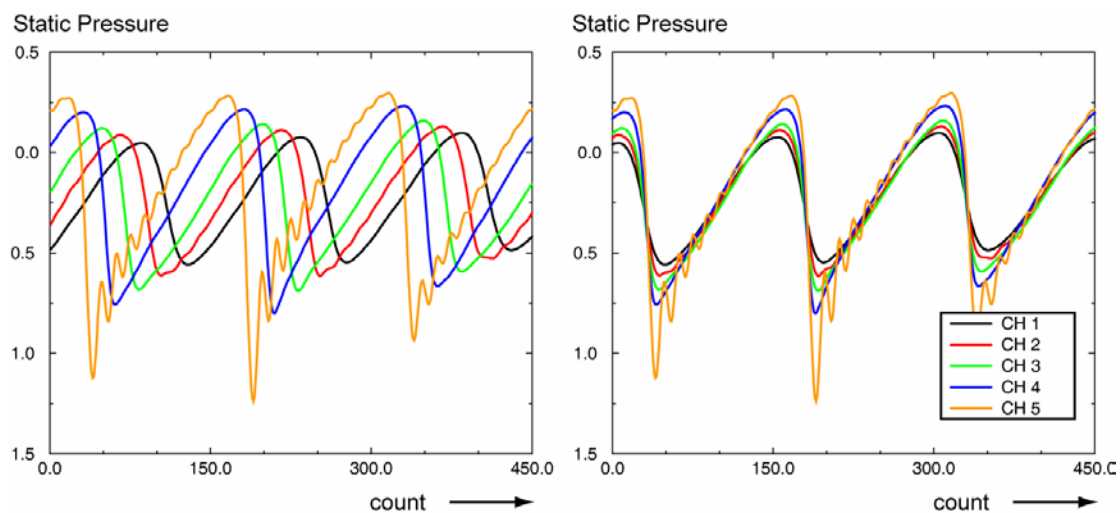


**Figure 27: Averaged Static Pressure at Measuring Position, Simultaneous Data (left) and “Time-Shifted” (right).**

Figure 28 shows a cutout of pressure field measurements and related standard deviation. For additional information a sketch of the impeller profile is added.

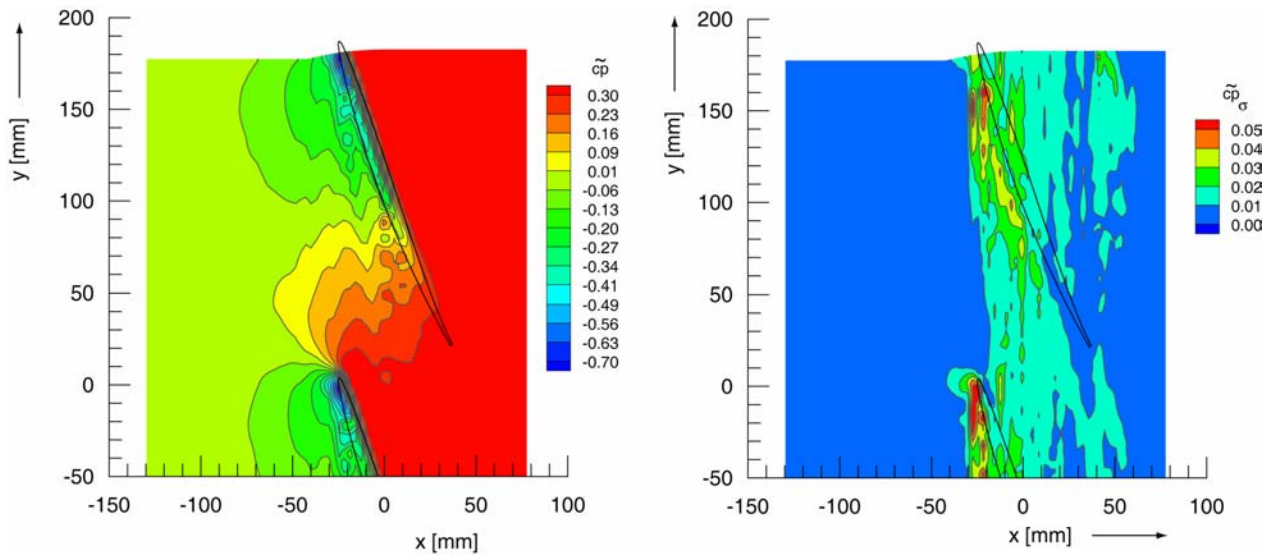


**Figure 28: Static Pressure and Related Standard Deviation at Wall Near Design Point of Pump [14].**

## 3.2.2 Detection of Rotating Components

When employing one single transducer, measurement of rotor flow is more or less limited to the stationary relative flow or to the periodical absolute flow.

Detection of non-synchronous components to impeller speed is possible with a second transducer or probe (Fig. 29) that is located in some circumferential distance  $\varphi$ . For the periodical (stationary relative) rotor flow the time-delay between measuring position  $p_1$  and  $p_2$  is given by

$$T = \frac{\hat{\varphi}}{2 \cdot \pi \cdot n} = \frac{\varphi}{360^\circ \cdot n}$$

where  $n$  [1/s] = impeller speed.

Calculation of cross-correlation function will help to detect non-synchronous components. The cross-correlation between two time signals  $p_1(t)$  and  $p_2(t)$  is given by

$$R_{12}(\tau) = \lim_{T \rightarrow \infty} \frac{1}{2T} \int_{-T}^T p_1(t) \cdot p_2(t - \tau) dt$$

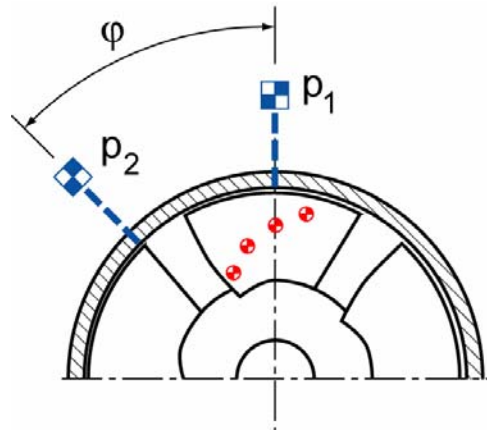


Figure 29: Detection of Rotating Components with Two Sensors.

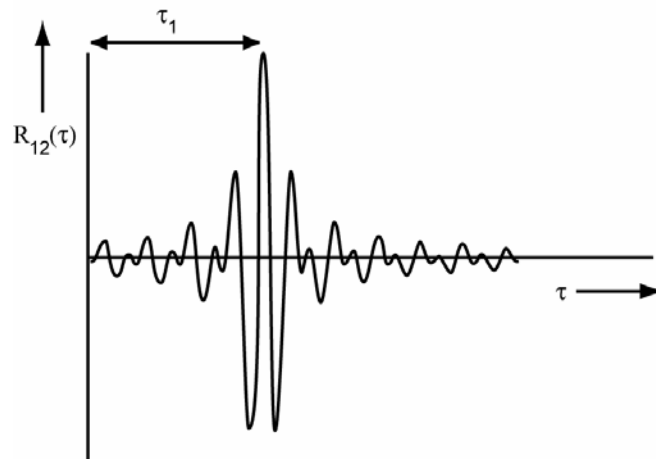


Figure 30: Cross-Correlation Function.

The peak value of  $R_{12}(\tau)$  occurs at  $\tau_1$  and is the time delay determined by the position of the two sensors and speed of the rotating component. Thus frequency of the rotating component is given by

$$f = \frac{1}{\tau_1} \cdot \frac{360^\circ}{\phi}$$

### Example: Investigation of Rotating Stall Inception

Figure 32 shows the pressure near the casing wall 5mm upstream of an axial flow impeller measured with two high response total pressure probes according to Fig. 31. Circumferential distance of probes is  $\phi = 45^\circ$ , signal of probe 2 is shifted to enhance readability. Rotor speed is  $n = 75$  Hz and the number of blades  $z = 16$  which results in a blade passing frequency of  $BPF = 1200$  Hz. Inception of rotating stall is indicated by spikes, until in less than 10 rotor revolutions fully developed rotating stall is reached [18]. More insight gives the cross-correlation of three time-windows in the bottom of Figure 32: Rotational speed at inception is around 50 Hz while fully developed stall rotates with 35 Hz.

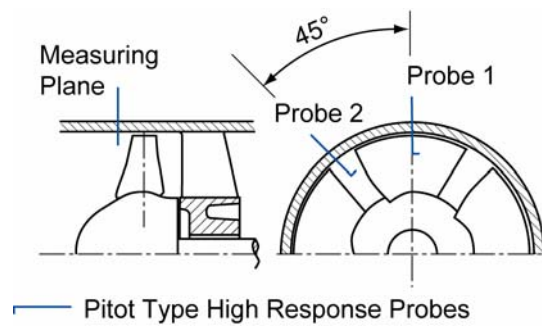


**Figure 31: Set-up for Detection of Rotating Stall.**

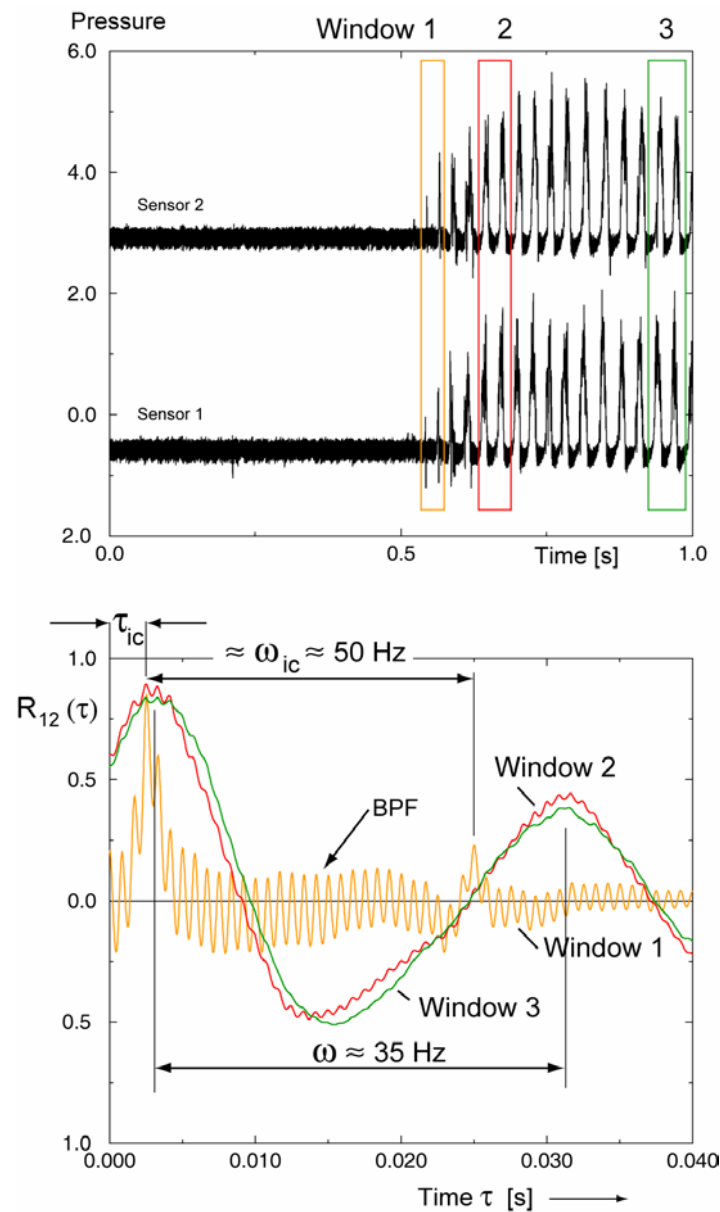


**Figure 32: Inception of Rotating Stall in Axial Flow Impeller. Time Signal (top) and Cross-Correlation for Time Windows (below).**

## 3.3 Investigation of Rotor Flow in Rotating Frame

When the relative flow in the rotor becomes unsteady in relation to the rotating frame itself or for example information on the pressure distribution along blades is requested, pressure transducers have to be fitted into rotating components. Figure 33 shows an eight-channel telemetry system for measurement of pressure distribution along impeller blades. Amplifier and VHF sender are mounted on the rotating shaft of the pump. The output of the pressure transducers is processed through a voltage frequency converter, frequency multiplexer and then transmitted wirelessly via the VHF sender (Fig. 34). The received signal is demodulated, passed through a frequency voltage converter, filtered and processed as analogue signal to the data acquisition system. Bandwidth of this system is around 2 kHz per channel.

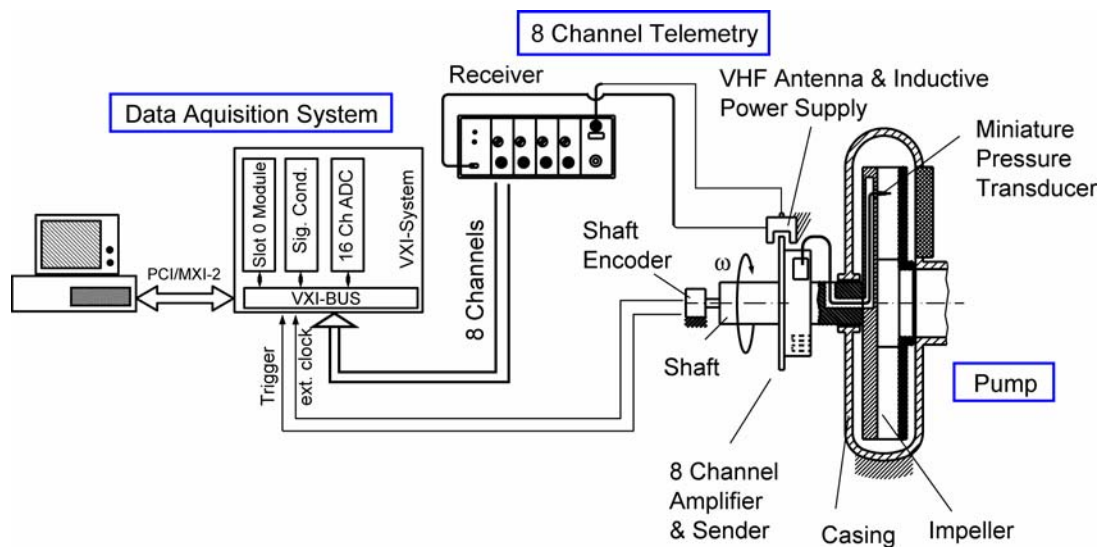


Figure 33: Telemetry System for Unsteady Pressure Measurements in Rotating Components.

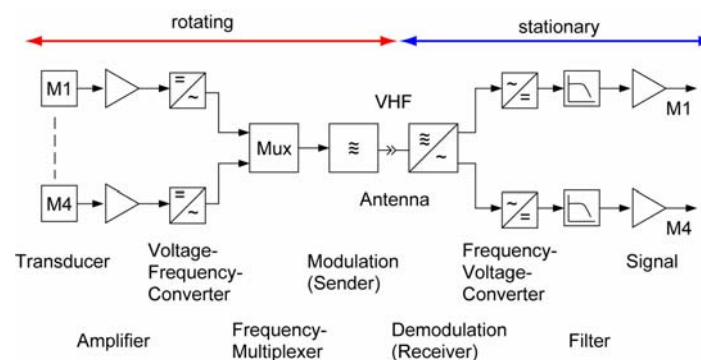


Figure 34: Schema of Telemetry Data Transmission.

### Example: Pressure Distribution on the Blades of a Radial Impeller

This example shows how to measure the pressure distribution along an impeller blade at various states of cavitation. A sketch of test rig is given in Fig. 35. A vane less radial diffuser is used as a discharge casing in order to generate an (averaged) uniform circumferential pressure distribution. The impeller consists of several components to enable easy installation of measurement technique. One blade (Fig. 36) is fitted with an insert containing 8 miniature pressure transducers. The cavity in front of each transducer is filled



with silicon oil to ensure high response. Front sealing is realised by a rubber plate while the sensor cables on the rear are lead through watertight tubes (details, see Fig. 8). Pressure can be measured on either side of the blade depending on which pressure tap is open. Since circular arc impeller blades are used, the position of the insert along the blade can easily be adjusted by rotating the adjustment plates (Fig. 36). Therefore a high resolution of measurement points along a blade is obtained. The telemetry system and data acquisition set-up follow Figure 33. A transparent impeller front plate and a window in the pump casing allow cavitation observation.

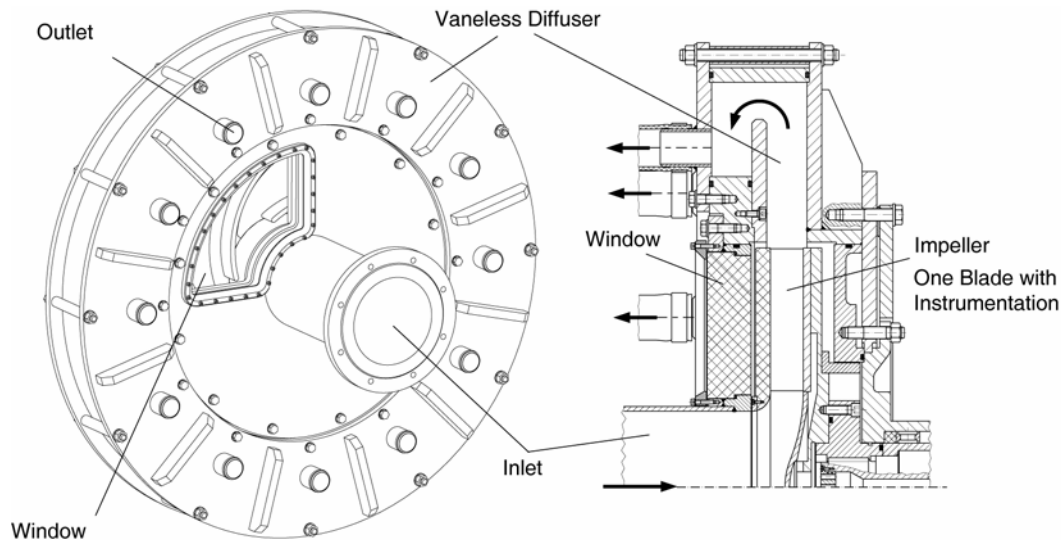


**Figure 35: Sketch of Test Rig for Radial Pump Impeller.**

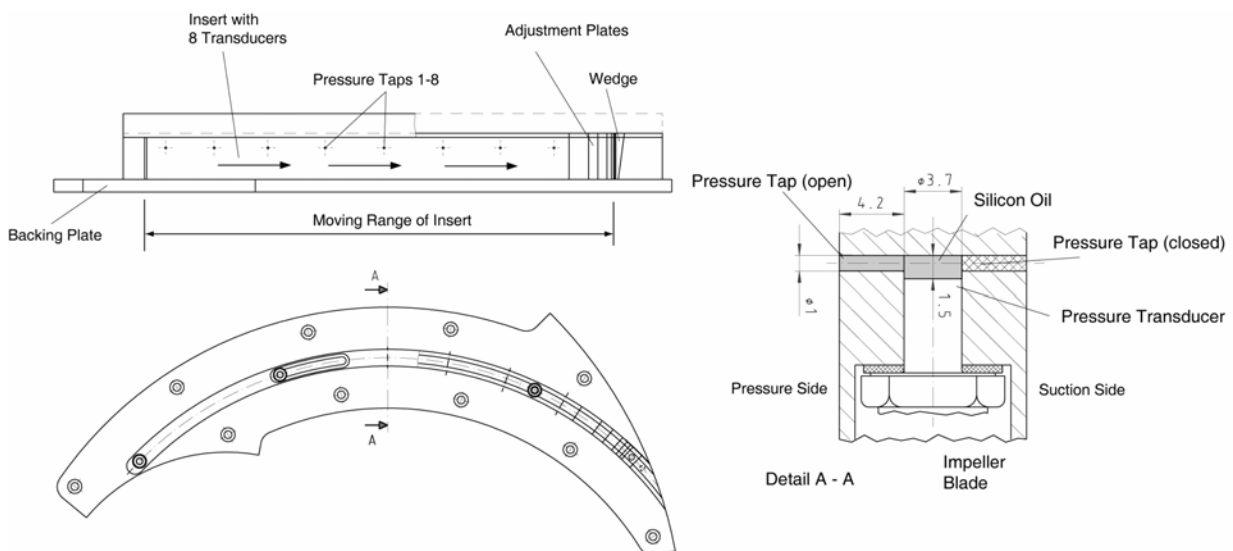


**Figure 36: Impeller Blade with Instrumentation (KULITE® XTM-XX-190M).**

Since thermal zero shift requires frequent balancing which may be difficult during tests, a preliminary calibration of thermal zero shift was made. In a pump with horizontal shaft a sinusoidal fluctuation can be observed during operation, which is caused by the variation of geodetic height and increases therefore proportional with radius of the measuring point. Figure 37 shows the fluctuating geodetic pressure for one



radius. Depending on the aimed results it may be necessary to correct this for all measurements with respect to angle of rotation.

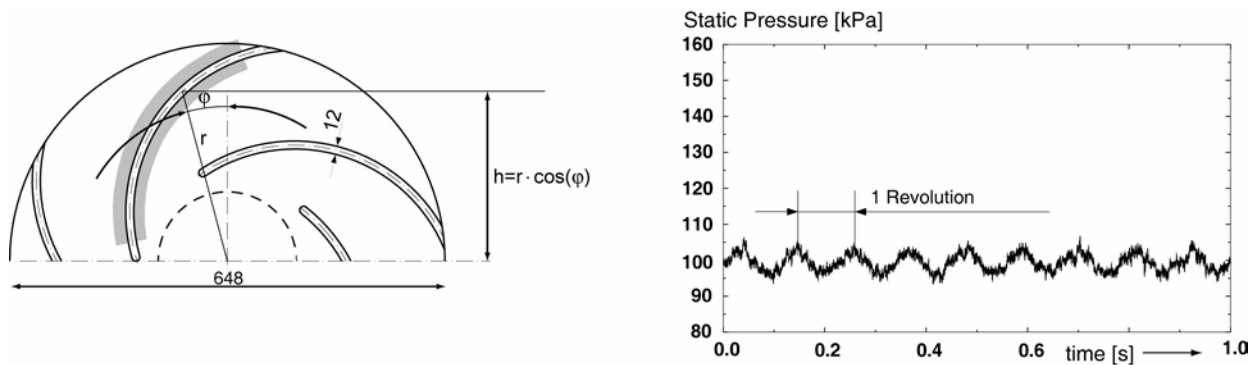


**Figure 37: Fluctuating Geodetic Head due to Impeller Rotation.**

Figure 38 compares measured and calculated pressure along a blade. A high resolution of measuring positions along the blade is achieved by the sliding insert, while no measurements can be made on leading and trailing edge of the blade with the used instrumentation.

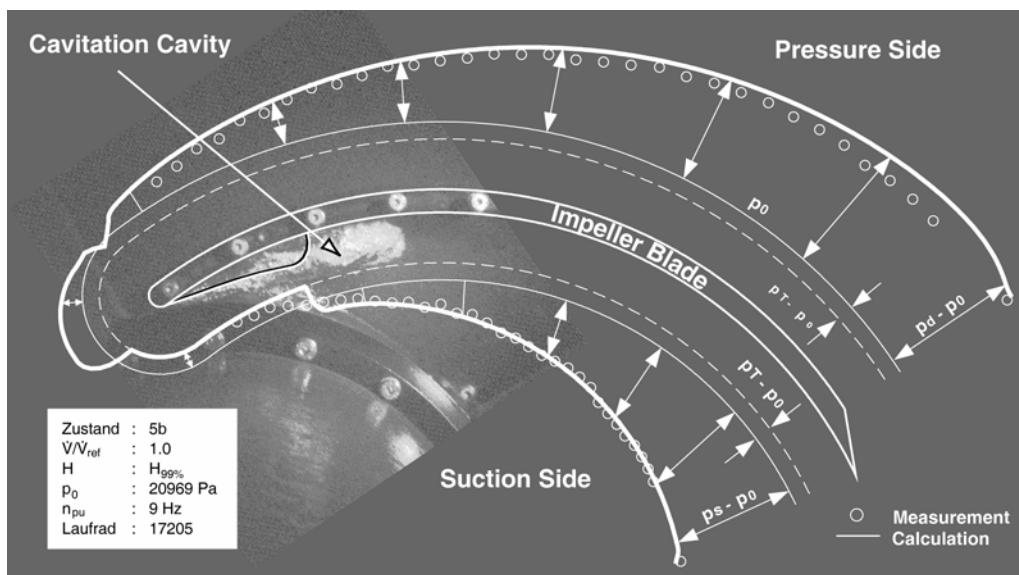


**Figure 38: Measured and Calculated Pressure Distribution on Impeller Blade [4, 5, 6].**

*Example: Pressure Distribution on the Blades of a Mixed-Flow Impeller*

Measurement of pressure distribution on the blades of a mixed-flow impeller is compared to a radial impeller more sophisticated because of the more complex geometry. Figure 39 shows a sketch of the investigated impeller and a picture taken during the installation process of miniature pressure transducers into the impeller blade. For this investigation KELLER® PA-2Mi sensors are employed, which are commonly used in the medical field. As Fig. 40 demonstrates, pressure on either side of the blade can be measured, depending on which pressure tap is open. The cavity in front of the transducer is filled with silicon oil; the diameter of the pressure taps of 1 mm ensures a good spatial resolution. Routing of transducer cables are in machined grooves which are filled with sealing compound afterwards to ensure

water tightness on the back of the transducer. Data acquisition by means of telemetry follows according to Fig. 33. An example of the achieved results is given in Fig. 41, which shows the pressure distribution on the suction side of a blade at a light state of cavitation. Rectangles indicate unsteadiness of static pressure expressed as standard deviation.



**Figure 39: Mixed-Flow Impeller with Miniature Pressure Transducers in Impeller Blade [8, 9].**

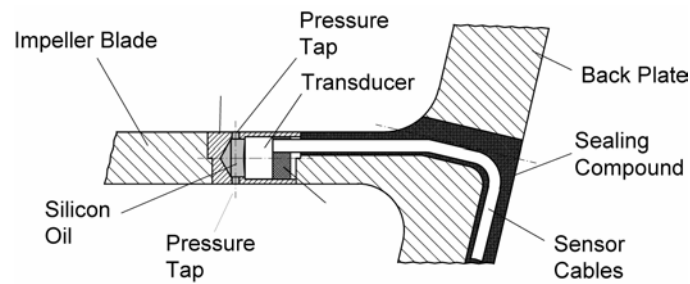


**Figure 40: Installation of Miniature Pressure Transducer (KELLER® PA-2Mi).**

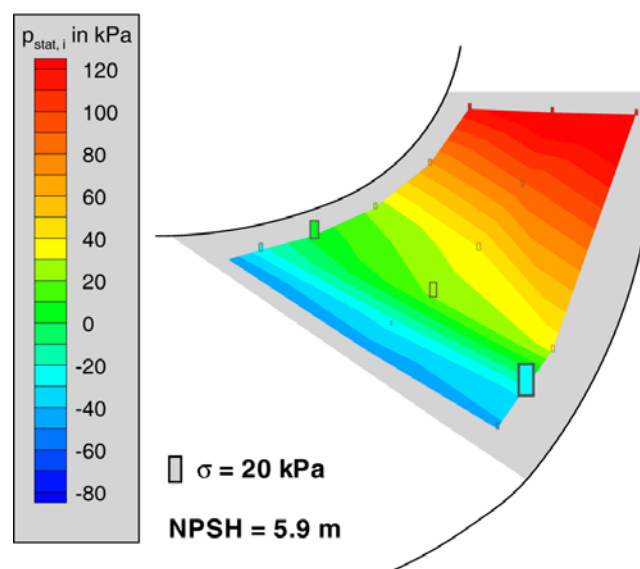


**Figure 41: Pressure Distribution on Suction Side at 0.8% Head Drop due to Cavitation [8, 9].**

## 3.4 High Response Probes

High response probes fitted with miniature pressure transducers are helpful when investigating the rotor exit flow. In contrast to non-intrusive techniques, which will deliver only velocity distributions, information on static as well as total pressure at rotor exit can be achieved. Probes equipped with multiple miniature pressure transducers for service in gas [13] or water [3] are widely used. Following the considerations of chapter 3.2, measurement of rotor exit flow from a stationary frame is more or less limited to the periodically relative flow. Since in most cases phase averaging will be necessary most measurements can also be made with single-hole probes fitted with one single pressure transducer. While multi-hole probes read data of all holes simultaneously a single-hole reads the data successively because it had to be adjusted to several angular positions to simulate a multi-hole probe. A single-hole probe is suitable for two-dimensional flows, with an additional probe separated peripherally, which pressure tap differs in inclination with respect to the machine axis, three-dimensional measurements can be made [19, 2]. Advantages of single-hole probes are: simple design, pressure transducers can be mounted near to tip to ensure good response, small size and low cost. The main disadvantage is its limitation to measurement of phase-averaged flow. Figure 42 shows a single-hole probe with spherical head and KULITE® XCQM transducer. The cavity in front of the transducers is filled with silicone oil to ensure good frequency response, which is around 8 kHz. Due to the rugged design the probe has been in service for several years, withstanding cavitation as well as velocities up to 30 m/s.

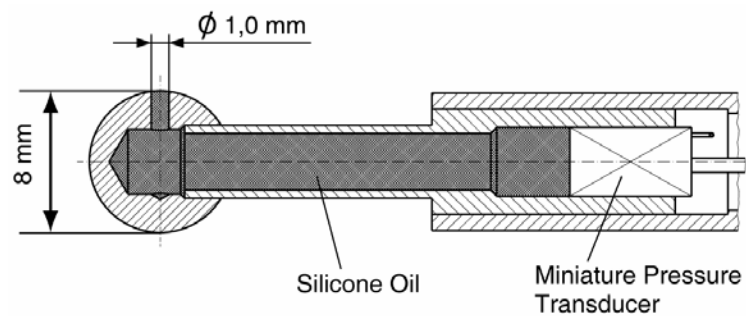


**Figure 42: Single Hole Probe Fitted with KULITE® XCQM Miniature Pressure Transducer for Measurements in Water (built at Pfleiderer-Institut TU Braunschweig).**

### 3.4.1 Single-Hole Probe

#### *Calibration of a Single-Hole Probe*

In order to obtain velocities and pressure from the probe readings, the probe is calibrated like a common hydraulic multi-hole probe. For calibration a uniform, steady water flow in a closed channel is required. Figure 43 shows the dimensionless pressure readings for different probe angles. The calibration curve corresponds to the well-known pressure distribution around a sphere. The measured pressure is equal to the static ambient pressure at a probe angle of  $\alpha_0 = \pm 44.6^\circ$ . For use of the calibration data, the probe output from Fig. 43 is approximated by a fourth-order Chebyshev-Polynomial. By use of this polynomial and the determined angle  $\alpha_0$  the maximum probe pressure  $p_t$  as well as the static pressure  $p_{st}$  can be calculated.

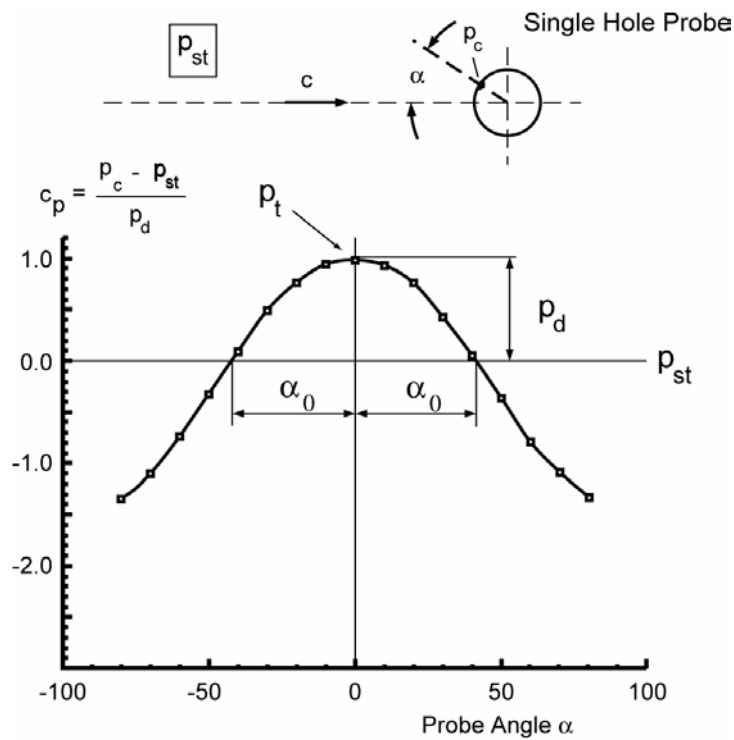


**Figure 43: Calibration of Single-Hole Probe.**

## *Measurements with a Single-Hole Probe*

Figure 44 demonstrates the procedure involved to derive the flow data from the pressure readings. The pressure readings for eight angular positions of the probe are shown in Fig. 44,a). These pressure readings are used to approximate a fourth-order polynomial. Total pressure is achieved directly from the polynomial at its maximum, while static pressure is acquired by looking for the intersection between the polynomial with a line in the length of two times  $\alpha_0$ . The fluid angle is found in the middle of  $\pm \alpha_0$ .

## Unsteady Pressure and Velocity Measurements in Pumps

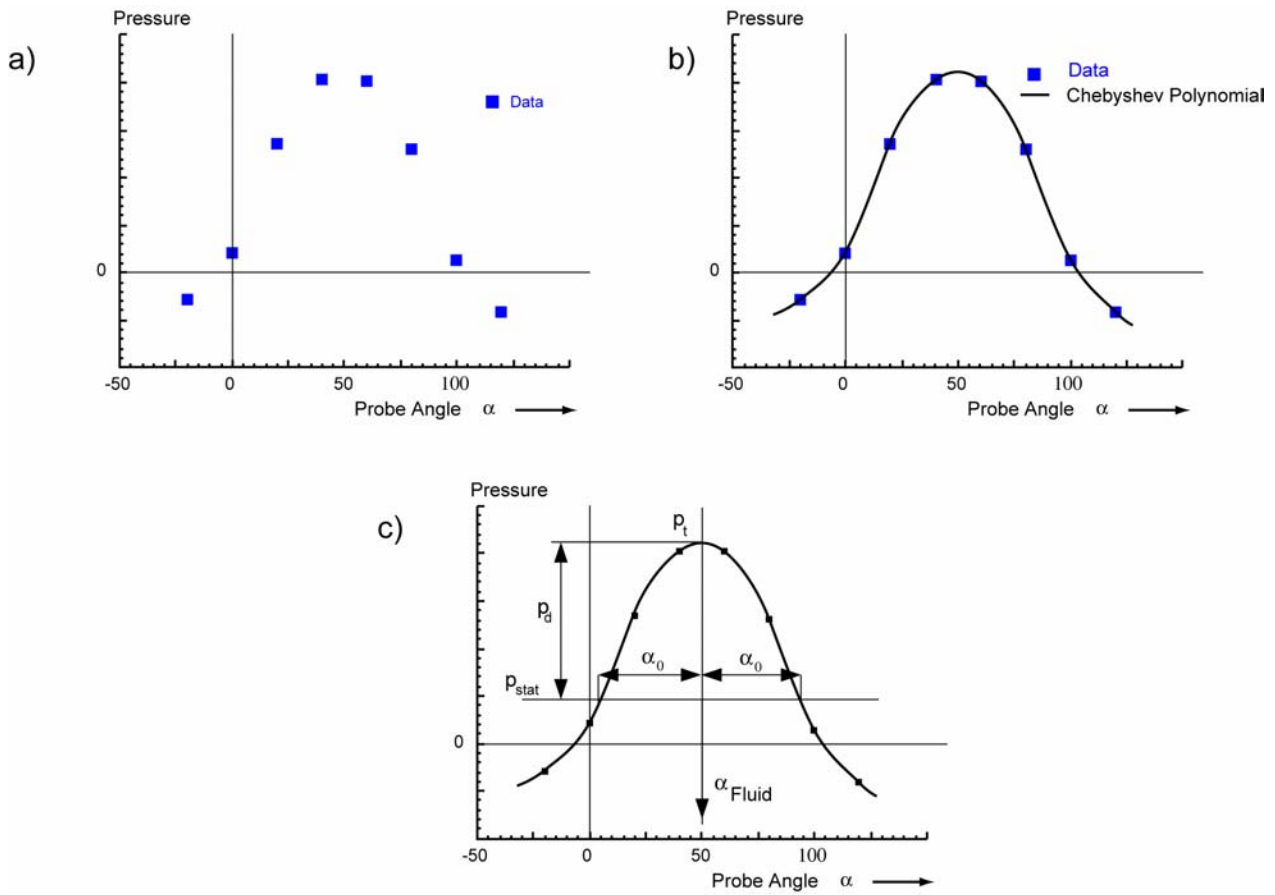


**Figure 44: Pressure Readings of a Single-Hole Pressure Probe and Procedure to Derive Flow Angle, Static and Total Pressure.**

### Inertia Effects

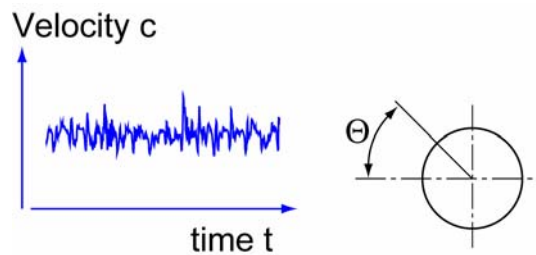


**Figure 45: Pressure Distribution around Sphere is Affected by Inertia Effects.**

Measurement of unsteady pressure by means of pressure probes is effected by inertia effects. According to a model derived from [15] for an inviscid theory the pressure distribution around a sphere can be expressed by

$$p(t, \Theta) = p_{st} + K_A(\Theta) \cdot \frac{\rho}{2} c^2(t) + K_B(\Theta) \cdot \rho \cdot r_{Probe} \cdot \frac{dc}{dt}$$

with

$$K_A(\Theta) = \frac{1}{4} \cdot (-5 + 9 \cdot \cos^2 \Theta)$$

$$K_B(\Theta) = \frac{3}{4} \cdot \cos \Theta \cdot (-3 + 5 \cdot \cos^2 \Theta)$$

where  $p_{st}$  = static pressure  
 $\rho$  = fluid density  
 $r_{probe}$  = probe head radius

$K_A(\Theta)$  is equal to the pressure distribution in steady, inviscid flow while  $K_B(\Theta)$  characterises the additional term generated by inertia forces. It follows from the equation that inertia effects increase with probe head radius and velocity gradient  $dc/dt$ . It is therefore advisable to choose the smallest probe head possible. As Figure 46 shows, neglecting inertia effects can cause big differences especially in the jet/wake region where velocity gradients become quite high. It should be mentioned that the averaged values derived from velocities in Fig. 46 are almost the same irrespective if inertia effects are included or not.

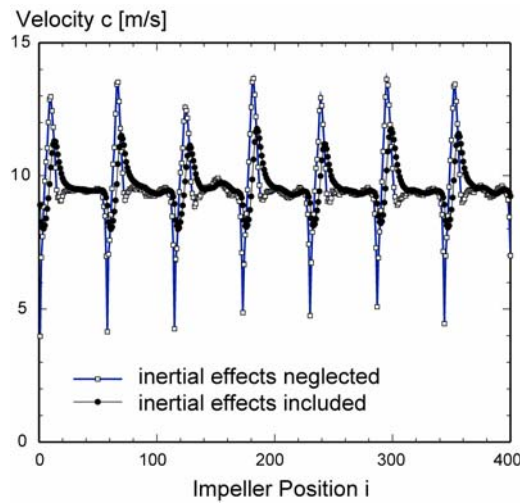


**Figure 46: Phase Averaged Velocity at Impeller Exit.**

## Measurement of Rotor Exit Flow

Schema of data acquisition set-up follows Fig. 26. For measurement of rotor exit flow (Fig. 47), the probe is adjusted to eight positions evenly spaced to the average flow angle. At each angular position the unsteady probe pressures are recorded over e.g. 80 rotor revolutions while the sampling rate is determined by the employed shaft encoder. After recording all eight data sets, each data set is averaged over 80 rotor revolutions to increase signal-to-noise ratio (chapter 3.1). Fourth order polynomials are fitted to the probe data. Figure 48 shows polynomials for 30 circumferential measuring positions. For each position static and total pressure as well as velocity and flow angle are obtained by the aforementioned procedure. As an example for the obtained results, the velocity and total pressure field at the exit of a mixed-flow pump impeller is given in Fig. 49.

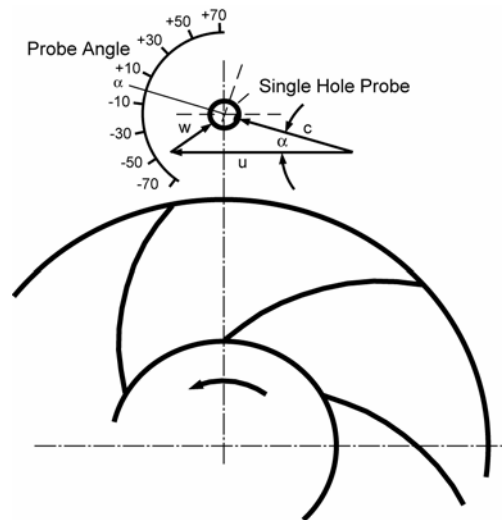


Figure 47: Set-up of Single-Hole Probe at Impeller Outlet.

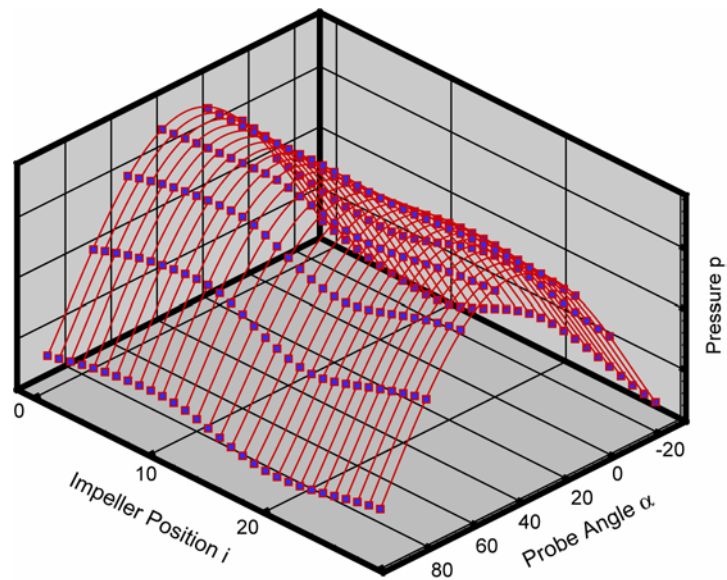
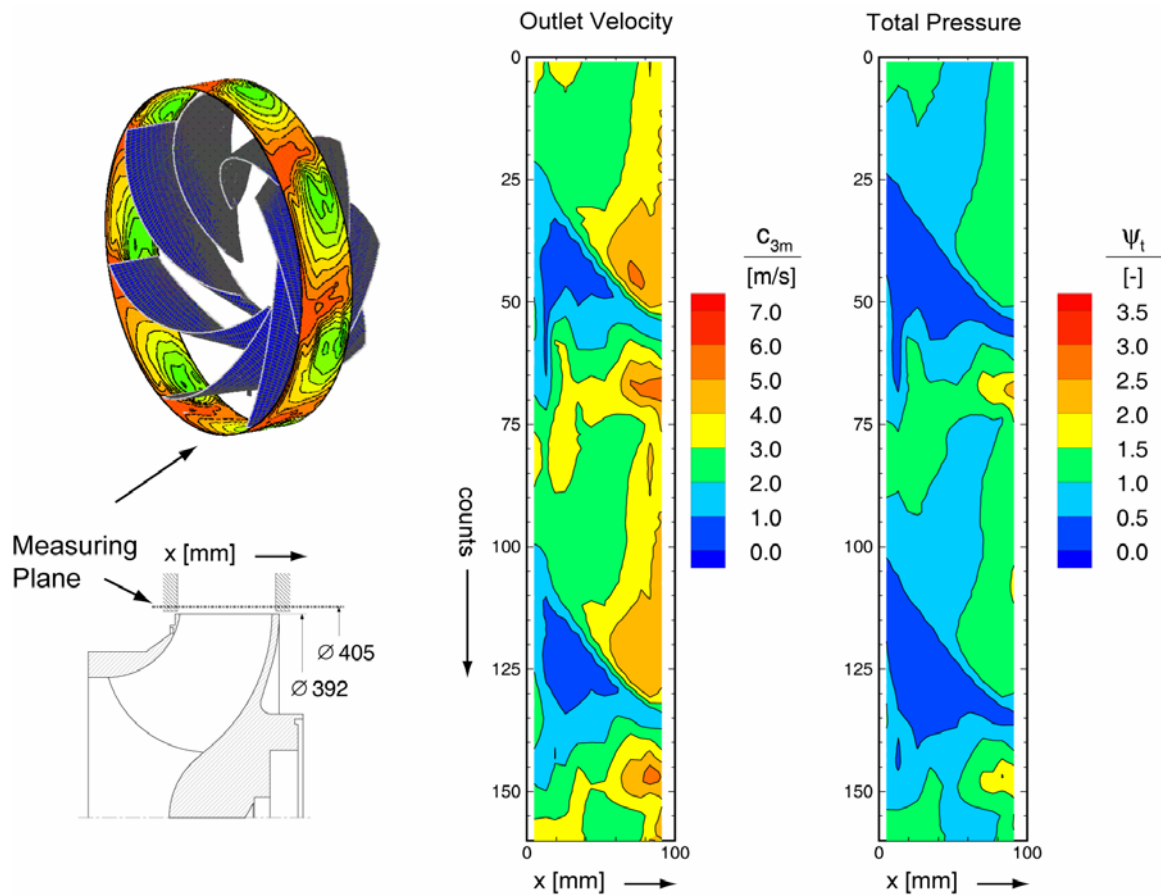


Figure 48: Averaged Pressures Fitted by Polynomials.





**Figure 49: Velocity and Total Pressure at Impeller Exit Measured with Single-Hole Probe.**

## 3.4.2 Measurements of 3-Dimensional Flow Using a Dual Probe Sampling Technique

When information on 3-dimensional, periodical rotor exit flow is required, the technique specified in chapter 3.4.1 can be enhanced by employing a dual probe sampling technique as described in [19, 2]. Figure 50 shows the arrangement in an axial flow pump as an example. In this case pitot-type probes are used, but sphere type probes may be used as well. In order to achieve information on the third component of velocity, second probe B is arranged in some circumferential distance  $\phi$  (Fig. 50). In contrast to probe A whose head is inclined by 90 deg relative to the shaft axis, the head of probe B is inclined by 45 deg (Fig. 51). As the calibration curves in Fig. 51 demonstrate, probe B is very sensitive to pitch angle  $\gamma$  while probe A is almost unaffected.



## Unsteady Pressure and Velocity Measurements in Pumps

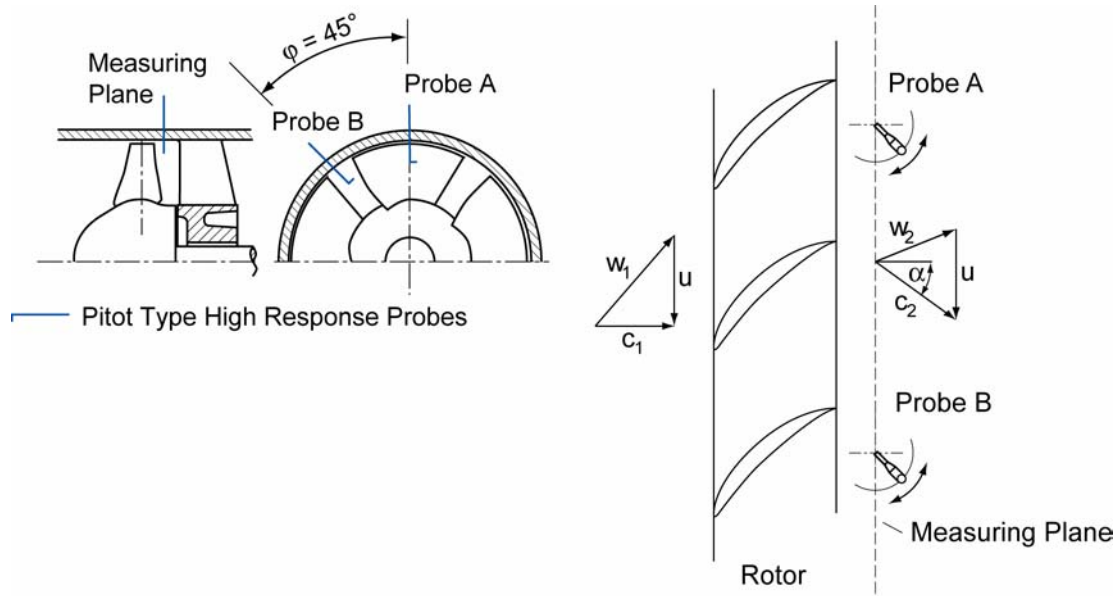


Figure 50: Arrangement of Probes in the Test Section.

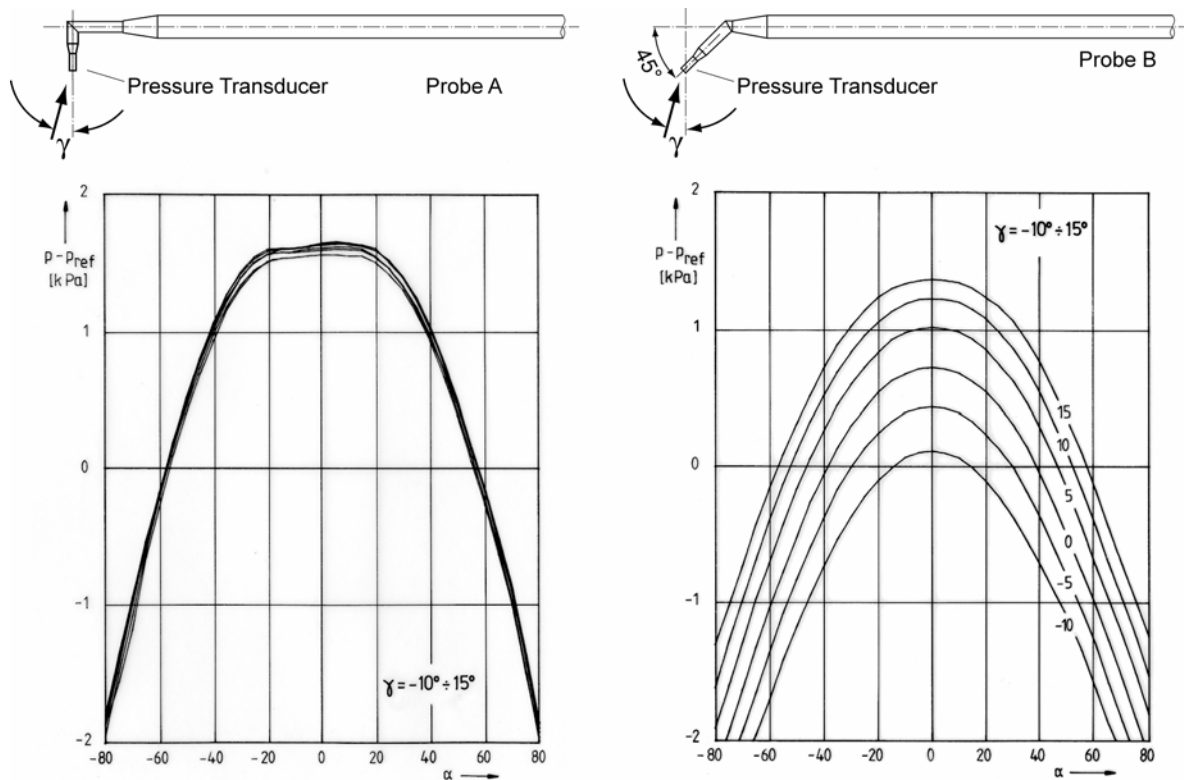


Figure 51: Calibration Data of Probe A and B for Different Pitch Angles  $\gamma$  [2].

Following steps does evaluation of probe readings with the dual probe technique:

- Recording simultaneous data of probe A and B
- Time shifting data from probe B to probe A (according to angle  $\phi$ )

- Calculation of ensemble phase averaged data
- Calculation of best fit polynomials (Fig. 52)
- Flow angle  $\alpha$  is determined directly from Fig. 52
- Total pressure and static pressure as a first approximation is derived from data of probe A
- Pitch angle  $\gamma$  and final values of pressure are derived by few iteration steps [2, 19]

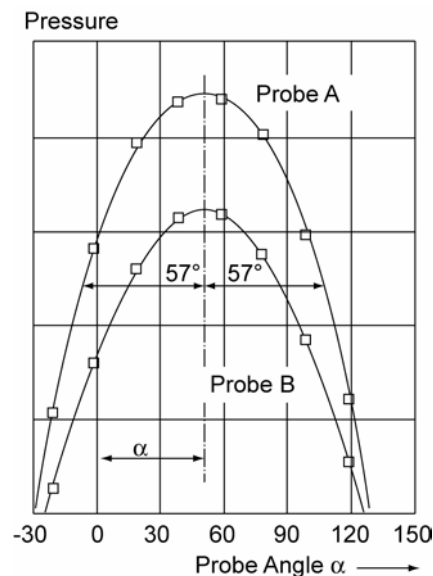


Figure 52: Phase Averaged Pressure Readings from Probe A and B over Probe Angle  $\alpha$  [2].

## 7.0 REFERENCES

- [1] Bendat, J.S., Piersol, A.G. (2000). Random Data, 3rd ed. New York: Wiley.
- [2] Brodersen, S., Wulff, D.L. (1992). Measurements of the Pressure and Velocity Distribution in Low-Speed Turbomachinery by Means of High-Frequency Pressure Transducers. ASME, J. of Turbomachinery, Vol. 114, pp. 100-107.
- [3] Castorph, D. (1975): Messung des instationären Strömungsfeldes einer Kaplan turbine mit elektrischen Miniatursonden. Forsch. im Ingenieurwesen, Vol. 41, No.6.
- [4] Dreiß, A. (1997). Untersuchung der Laufradkavitation einer radialen Kreislumpumpe durch instationäre Druckmessungen im rotierenden System. Mitteilungen des Pfeleiderer-Instituts für Strömungsmaschinen, Heft 5, Sept. 1997, pp. 1-102, Dissertation TU Braunschweig 1997, Verlag und Bildarchiv W. H. Faragallah.
- [5] Dreiß, A.; Kosyna, G. (1997): Experimental Investigations of Cavitation-States in a Radial Pump Impeller. JSME CENTENNIAL GRAND CONGRESS Proceedings of International Conference on Fluid Engineering, Vol 1, pp. 231-238 Tokyo, Japan: July 13-16, 1997, JSME.
- [6] Dreiß, A.; Kosyna, G. (1997): The Influence of Unsteady Cavitation Effects on the Shape of NPSH-Head-Drop-Curves. Proceedings of the 2nd JAPANESE-GERMAN SYMPOSIUM on Multi-Phase Flow Tokyo, Japan: September 25-27, 1997, pp. 435-446, JSPS.

## Unsteady Pressure and Velocity Measurements in Pumps

---

- [7] Endevco (ca. 1980). Textbook for short course “Dynamic Pressure Measurements”. Endevco Corp. San Juan Capistrano, CA.
- [8] Friedrichs, J. (2003). Auswirkungen instationärer Kavitationsformen auf Förderhöhenabfall und Kennlinieninstabilität von Kreiselpumpen. Mitteilungen des Pfeiderer-Instituts für Strömungsmaschinen, Heft 9, März 2003, 185 S., Dissertation TU Braunschweig 2003, Verlag und Bildarchiv W. H. Faragallah.
- [9] Friedrichs, J.; Kosyna, G. (2002). Experimental and Numerical Investigation of the Performance Instability in a Mixed-Flow Impeller. Proceedings of ASME FEDSM'02. 2002 ASME Fluids Engineering Division Summer Meeting, Montreal, Canada, July 14-18, 2002. FEDSM2002-32326.
- [10] Goldstein, R.J. (Ed.) (1983). Fluid Mechanics Measurements. 1st ed. New York, Hemisphere Publ. Corp.
- [11] Goltz, I. (2006). Entstehung und Unterdrückung der Kennlinieninstabilität einer Axialpumpe. Mitteilungen des Pfeiderer-Instituts für Strömungsmaschinen, Dissertation TU Braunschweig 1995, Verlag und Bildarchiv W. H. Faragallah (in preparation).
- [12] Gossweiler, C.R., Kupferschmied, P., G. Gyarmathy (1995): On Fast-Response Probes: Part 1 – Technology, Calibration, and Application to Turbomachinery. ASME J. of Turbomachinery, Vol. 117, pp. 611-617.
- [13] Kerrebrock, J.L., Epstein, A.H., Thompkins, W.T. (1980) A Miniature High Frequency Spehre Probe. in Measurement Methods in Rotating Components of Turbomachinery, pp. 91-97. Joint Fluids Engineering Gas Turbine Conference, New Orleans, March 10-13, 1980. New York, ASME.
- [14] Kosyna, G.; Goltz, I.; Stark, U. (2005). *Flow Structure of an Axial-Flow Pump from Stable Operation to Deep Stall*. FEDSM2005-77350, 2005 ASME Fluids Engineering Summer Conference, Houston Texas, USA, June 19-23, 2005.
- [15] Kovasznay, L.S.G., Tani, I., Kawamura, M., Fujita, H. (1981). *Instantaneous Pressure Distribution Around a Sphere in Unsteady Flow*. ASME, J. of Fluids Engineering, Vol. 103, pp. 497-502.
- [16] Lakshminarayana, B., Poncet, A. (1974), *A Method of Measuring Three-Dimensional Wakes in Turbomachinery*. J. Fluids. Engr., Trans. ASME, Vol. 96, No. 2, June 1974, pp. 87-91.
- [17] Lakshminarayana, B. (Ed.) (1980). *Measurement Methods in Rotating Components of Turbomachinery*. Joint Fluids Engineering Gas Turbine Conference, New Orleans, March 10-13, 1980. New York, ASME.
- [18] Saathoff, H.; Deppe, A.; Stark, U.; Rohdenburg, M.; Rohkamm, H.; Wulff, D.; Kosyna, G (2002): *Steady and Unsteady Casingwall Flow Phenomena in a Single Stage Low Speed Compressor at Part-Load Conditions*. 9th International Symposium on Transport Phenomena and Dynamics of Rotating Machinery, February 10-14, 2002, Honolulu, Hawaii, USA.
- [19] Shreeve, R.P., Neuhoﬀ, F. (1984). *Measurements of the Flow From a High-Speed Compressor Rotor Using a Dual Probe Digital Sampling (DPDS) Technique*. ASME, J. f. Gas Turbines and Power, Vol. 106, pp. 366-375.